QATAR UNIVERSITY

Graduate Studies

College of Arts and Sciences

Surface characterization and luminescence properties of AlN doped with RE elements (Sm, Ho, Gd, Tm)

A Thesis in Materials Sciences and Technology

By

Ismail Ayodele Balogun

Copyright 2015: **Ismail Balogun**

Submitted in Partial Fulfillment of the Requirements for the Degree of
Master of Science

June 2015

Declaration

To the best of my knowledge, this thesis contains no material previously published or written by another person or institution, except where due reference is made in the text of the thesis. This thesis contains no material which has been accepted for the award of any other degree in any university or other institution.

Name: Ismail Ayodele Balogun

Signature: Date: 08-06-2015

The thesis of **Ismail Ayodele Balogun** was reviewed and approved by the following:

We, the committee members listed below accept and approve the Thesis of the student named above. To the best of this committee's knowledge, the Thesis conforms the requirement of Qatar University, and we endorse this thesis for examination.

Advisor:
Name ____Dr. Khaled Youssef___________________________________

Signature ____ Date__________

Committee member:
Name ____Dr. Khalid Al Saad_____________________________________

Signature ____ Date__________

Committee member:
Name ____Dr. Ahmad Ayesh______________________________________

Signature ____ Date__________

External examiner:
Name ____Dr. Ahmed Abdalla_____________________________________

Signature ____ Date__________

Abstract

Rare- earth (RE)-doped III-nitride broad band-gap semiconductors have attracted enormous interest as a foundation for optoelectronics devices, which combine the unique luminescence feature of Rare-earth ions with the electronic properties of the semiconductors. Recent progress toward nitride-based light emitting diode and light-emitting due to electric current devices have been made using crystalline and amorphous AlN and GaN doped with a different lanthanide elements. The Rare-earth ions' electronic structures are differ from the other elements and are unique due to an incompletely filled $4F^n$ shell. The 4*F-orbital* electrons lay inside the ion and are protected from the surroundings by the filled $5S^2$ and $5P^6$ electron orbitals. When these rare-earths doped are excited by any external means, intense sharp-line emission is observed due to intra-$4F^n$-shells transitions of the rare-earth ion core.

In the present work, sputtered deposited thin films of AlN doped with rare-earth elements (Sm, Ho, Gd, Tm) are investigated for their structures, luminescence and spectroscopic properties. Thin films were deposited at various temperatures.

X-ray diffraction (XRD) analysis was performed for structural analysis and crystallite size calculation in crystalline films. Scanning electron microscopy was also used to confirm the information obtained from XRD. Luminescence and spectroscopic analysis were performed using photoluminescence tool and Fourier transform infra-red. The effect of the temperature on the surface morphology and luminescence properties was also studied. Energy dispersive x-ray analysis was performed on the films to find the constituents and

impurities in the samples. Atomic force microscopy was also used for determination of surface roughening, and thermal gravimetric analysis was used to investigate loss of mass of the samples over a range of temperature.

This work provides investigations of these materials for their use in photonic and microelectronic devices.

Table of Contents

Page

List of Figure viii

List of Tables x

List of Abbreviations xi

Acknowledgement xiii

Dedication xiv

Chapter 1

1. Introduction 1

Chapter 2

2. Literature review 5

2.1 Aluminum nitride thin film 5

2.1.1 Introduction 5

2.2 Crystal structure of Aluminum nitride 6

2.3 Thermal and chemical properties 7

2.4 Electrical properties 8

2.5 Mechanical properties 8

2.6 Optical properties 9

2.7 Doping and luminescence of AlN with rare-earth elements 12

2.8 RF magnetron sputtering 15

Chapter 3

3. Experimental set-up and Techniques 18

3.1 Films growth and substrate temperature 18

3.2 Characterization techniques 19

3.2.1 X-ray diffraction (XRD) 19

3.2.2 Scanning electron microscopy (SEM) 21

3.2.3 Energy dispersive X-ray (EDX) 22

3.2.4 Atomic force microscopy (AFM) 23

3.2.5 Fourier transform infrared (FTIR) 24

3.2.6 Thermal gravimetric analysis (TGA) 26

3.2.7 Photoluminescence 27

3.2.7.1 CIE colour coordinate 28

Chapter 4

4. Results and Discussion 30

4.1 Structural Characterization 30

4.1.1 X-ray diffraction 30

4.1.2 Scanning electron microscopy/Energy dispersive X-ray ... 34

4.1.3 Atomic force microscopy 39

4.1.4 Fourier transform infrared 44

4.1.5 Thermal gravimetric analysis 47

4.2 Luminescence 49

4.2.1 Photoluminescence 49

Chapter 5

5. Conclusion 55

6. Future work 56

7. References 57

List of figures

Page

Figure 2.1a Hexagonal closely-packed structure of wurtzite AlN 7
Figure 2.1b [AlN_4] tetrahedral units stacking along the [001] direction 7
Figure 2.2 Diagrammatical set up of magnetron sputtering system 17
Figure 3.1 Schematic diagram of RF magnetron sputtering system 19
Figure 3.2 Schematic diagram of the XRD basics 21
Figure 3.3 Quanta 200 SEM/EDX system used in the study 23
Figure 3.4 Atomic force microscope used in the study 24
Figure 3.5 Transmission FTIR spectra: (a) The original AlN powder before electrophoretic deposition; (b) The AlN film scraped from the Al cathode 25
Figure 3.6 Thermogravimetric curves of the AlN samples without or with the presence of phosphates with different added amounts of sintering aids and organic specimens: (a) obtained at a heating rate of 2°C/min; (b) obtained at a heating rate of 10°C/min 26
Figure 3.7 Maple II photoluminescence tool used in this study 28
Figure 3.8 The CIE chromaticy diagram 29
Figure 4.1a XRD spectrum of sample Sm/-196 32
Figure 4.1b XRD spectrum of sample Gd/250 32
Figure 4.1c XRD spectrum of sample Gd/450 33
Figure 4.1d XRD spectrum of sample Ho/700 33
Figure 4.2a SEM micrograph of sample Sm/-196 35
Figure 4.2b EDX spectrum of sample Sm/-196 35
Figure 4.3a SEM micrograph of sample Gd/250 36
Figure 4.3b EDX spectrum of sample Gd/250 36
Figure 4.4a SEM micrograph of sample Gd/450 37
Figure 4.4b EDX spectrum of sample Gd/450 37
Figure 4.5a SEM micrograph of sample Ho/700 38
Figure 4.5b EDX spectrum of sample Ho/700 38
Figure 4.6 (a) 2-D morphology (b) 2-D sensor retrace (c) Z sensor retrace. (d) 3-D morphology of sample Sm/-196 40
Figure 4.7 (a) 2-D morphology (b) 2-D sensor retrace (c) Z sensor retrace. (d) 3-D morphology of sample Gd/250 41
Figure 4.8 (a) 2-D morphology (b) 2-D sensor retrace (c) Z sensor retrace. (d) 3-D morphology of sample Gd/450 42
Figure 4.9 (a) 2-D morphology (b) 2-D sensor retrace (c) Z sensor retrace. (d) 3-D morphology of sample Ho/700 43

Figure 4.10a FTIR graph of sample Sm/-196 45
Figure 4.10b FTIR graph of sample Gd/250 45
Figure 4.10c FTIR graph of sample Gd/450 46
Figure 4.10d FTIR graph of sample Ho/700 46
Figure 4.11a TGA graph of sample Sm/-196 47
Figure 4.11b TGA graph of sample Gd/250 48
Figure 4.11c TGA graph of sample Gd/450 48
Figure 4.11d TGA graph of sample Ho/700 49
Figure 4.12 Electron configurations for (a) a singlet ground state; (b) a singlet excited state; (c) a triplet-excited state 50
Figure 4.13 Photoluminescence spectrum of Sm/-196 excited with 532 nm laser 53
Figure 4.14 Photoluminescence spectrum of Ho/700 excited with 532 nm laser 53
Figure 4.15 Photoluminescence spectrum of AlN: Tm excited with 530 nm laser performed at Ball state university, Indiana USA 54
Figure 4.16 Photoluminescence spectrum of AlN: Tm excited with 783 nm laser performed at Ball state university, Indiana USA 54

List of Tables

Page

Table 2.1 Basic properties of AlN at 300K 10
Table 3.1 EDAX parameters used in the study 22
Table 4.1 Doped AlN samples used in this study 30
Table 4.2 Surface roughness of the thin film samples 39
Table 4.3 Photoluminescence results of the samples 52

List of Abbreviations

RE	Rare earth
RE+3	Trivalent rare-earth ion
AlN	Aluminum nitride
Sm	Samarium
Ho	Holmium
Tm	Thulium
XRD	X-ray diffraction
SEM	Scanning electron microscopy
EDX	Energy dispersive X-ray
FTIR	Fourier transform infra-red
TGA	Thermo gravimetric analysis
PL	Photoluminescence
PLE	Photoluminescence excitation
CIE	International commission on illumination
GPa	Giga Pascal
Er	Erbium
XPS	X-ray photoelectron spectroscopy
GaN	Gallium nitride
AlGaN	Aluminum Gallium nitride
InN	Indium nitride
InAlN	Indium Aluminum nitride
RF	Radio frequency
UV	Ultraviolet
IR	Infra-red
nm	nanometre
III	Group three
V	Group five

LED	Light emitting diode
AlN: Ho	Aluminum nitride doped with Holmium
AlN: Sm	Aluminum nitride doped with Samarium
AlN: Gd	Aluminum nitride doped with Gadolinium
AlN: Tm	Aluminum nitride doped with Thulium
Ω	Ohm
α	Thermal expansion coefficient
κ	Thermal conductivity
eV	Electronvolt

Acknowledgement

With the successful completion of this endeavor, it will be nice to acknowledge those people who assisted in one way or the other in reaching this milestone.

Firstly, I indeed very grateful to my able Advisor Dr. Khaled Youssef, for his assistance and guidance during the course of this research. Your effort, time and patience you offered me during the course of this research guide me to the successful ending. Thank you for your unrestricted succor and cooperation, without you, no end in sight.

My sincere expression of gratitude also goes to Prof. Mariam A. Al madeed, head of the materials science and technology- master program, for her help in many aspects of my program. I have learnt a lot from her.

I am also thankful to all my lectures, supporting staff of the program and my committee members for their cooperation and helpful suggestions.

At last but not least I appreciate the support and prayers of Ummu Muhammad, Ummu Muhsin, friends and family. May Allah (swt) reward you abundantly.

Dedication

This work is dedicated to my father and my deceased mother who were the fundamental source of my achievement in life. All my achievements, honours, distinctions and knowledge are due to their love, affection, prayers, advices, guidance and brought up. My parents, if I keep saying thanks to you till eternity that is not even enough to compensate your love, but I say ‘May Allah (swt) reward you abundantly for the living one in this life and both of you in hereafter.

Chapter 1

Introduction

Aluminum nitride (AlN) is a direct wide band-gap III-V binary semiconductor which involves one element from the III group and one from the V group of the periodic table. Its appealing properties are responsible for the considerable attention of the scientific research community. Crystalline AlN thin film with wurtizite structure is employed in variety of applications like optical hard coatings, wear resistant and high temperature microelectronics. Some of these desirable properties also make AlN promising material for use in deep (UV) optoelectronics, surface acoustic wave devices, sensor and thin film resonators. Thermal conductive AlN films with moderate dielectric constant are considered for metal-Oxide semiconductor (MOS) application in corrosive and high temperature environments.[2,3,4,] Owing to the unique and famous optical and luminescence properties of Rare-earth elements that belong to lanthanides, they are becoming increasingly important in optoelectronic devices used in the alternative energy, defense, and communication industries. Mostly, they serve as phosphors and catalysts when incorporated in glass, ceramic or semiconductors. One of the most amazing properties of semiconductors, particularly wide band gap III-V semiconductors, like Aluminum nitride (AlN), is the light emission, which make them one of favorite hosts to exploit the optical and luminescence properties of rare-earth metals, which has revolutionized the photonics and optoelectronics fields. The wide band-gap semiconductor has been seen as highly potential candidate for blue and ultraviolet wavelengths optoelectronics.[6]

By using nitride emitters as pumps, all primary and mixed colors can be obtained. Generally rare-earths incorporated into III–nitride semiconductors were of the opinion of residing at isoelectronic substitutional sites. These sites are referred to as trap centers due to the strong interaction between incompletely filled 4*F-orbital* shells of the rare-earth ions and free carriers. Rare-earth traps in host lattices have relatively large carrier capture cross-sections but the facts about their structure are yet to be understood properly. Their large carrier capture cross-sections make bound excitons formation easier through Columbic interaction between trapped and free carriers.[14]

Research work have been carried out on rare-earth doped AlN, most of them have shown luminescence and optical properties of the doped AlN with elements like Erbium, Praseodymium, Gadolinium and Samarium in ultraviolet, visible and near infra-red regions. Most of these researches concentrated more on the luminescence and optical properties; and they had already established the fact that both amorphous and crystalline films could be used to produce luminescence in these doped films, but there is no significant work on how the deposition temperature affects these rare-earth doped AlN thin films structures properties and luminescence.

In the present work, sputtered deposited thin films of AlN doped with rare-earth elements (Sm, Ho, Gd, Tm) were investigated for their structure, luminescence and spectroscopic properties. Thin films were deposited at various temperatures. X-ray diffraction analysis was performed for structural analysis and grain size calculation in

crystalline films. Scanning electron microscopy of the films was performed to confirm the information obtained from XRD. Luminescence and spectroscopic were carried out using a photoluminescence technique. The effect of temperature on the surface morphology and luminescence property were investigated. Energy Dispersive X-ray measurements were performed to find the constituents and impurities in the samples.

The objective of this research is to study the effect of deposition temperature and corresponding film structure on the properties of the rare-earth doped AlN.

Organization of this thesis is as follows: chapter 2 is a theoretical background material to the experimental investigation. Crystal structure as well as electrical, thermal and chemical, mechanical and optical/luminescence properties of the aluminum nitride are comprehensively reviewed. The crystal structure, surface roughness and optical/luminescence are particular area of interest. Growth of the aluminum nitride thin film and its doping are also briefly reviewed.

In chapter 3, the experimental set-up and techniques are discussed. These involve discussion about RF magnetron sputtering, film growth and condition, characterization tools and luminescence tool employed in the study. The characterization tools are X-ray diffraction (XRD), scanning electron microscopy/energy dispersive X-ray (SEM/EDAX), atomic force microscopy (AFM), Fourier transform infrared spectroscopy (FTIR), photoluminescence and thermo gravimetric analysis (TGA).

Chapter 4 contains the results and discussion of the experimental works. It shows the micrographs of the characterization tools and the photoluminescence spectral of the films

when activated with a laser of 532nm. In the Discussion of the experimental result, explanation is made on how the deposition temperature affects the crystallinity of the films, roughness and particle size while being amorphous or crystalline does not hinder the doped films from emitting light when activated with laser in luminescence studies. The final chapter is dedicated to conclusions and future studies of the samples.

Chapter 2: Literature Review

2.1 Aluminum Nitride Thin Film

2.1.1 Introduction

Aluminum nitride is a wide gap semiconductor having potential application in deep ultraviolet (UV) optoelectronics and high power electronics devices. It has a history of over 120 years when it was first synthesized but it found its potential applications in microelectronics around 30 years ago. Aluminum nitride (AlN) is an III–V compound with a hexagonal wurtzite crystal structure that recently gained interest for its piezoelectric and photoelectric in addition to its applications in electronics. Among group III nitrides, comprises gallium nitride (3.4eV), indium nitride (1.9eV) and aluminum nitride (6.2eV), It has the largest band gap, which makes it an essential material when pursuing short wavelength of light emission devices.[6,7,11]

AlN is a covalent bonded material that has attractive properties for field emission applications because of its low-electron affinity, good dielectric property, thermal stability and non-reactive with convectional semiconductor process chemicals and gases.[7] In addition, it is desirable for its chemical stability, high thermal conductivity, low thermal expansion coefficient which is close to that for silicon, mechanical strength combined with, non-crystalline form, a reasonable compatibility to silicon and other III-V semiconductors, which makes it adaptable to a large variety of environments and enables great freedom in its device fabrication, such as in electrical packaging and composites.[6,7] However, much of

the attention of the AlN arises as a result of ternary and quaternary alloy formations with GaN to give AlGaN; and with InN to produce InAlN. The formation of AlGaN has allowed electronic and optical devices based on AlGaN/GaN fabrication.[7]

Investigation of uncontaminated AlN is not so easy to carry out, due to the high reactivity of aluminum with oxygen in the growth vessel.[7] Contamination-free deposition environments coupled with advanced procedures have recently been possible which now allowed researchers to consistently grow improved-quality AIN.[6,7]

2.2 Crystal structure of aluminum nitride

Aluminum nitride is one of the most versatile III–V compounds, synthesized from abundant elements aluminum and nitrogen. When crystallized in the hexagonal wurtzite structure, is a covalently bonded material with point group of C_{6v} and space grouping of $P6_3mc$. The *c/a* ratio of this point-group and space grouping is 1.333. 3.110 to 3.113 Å is the value of *a* parameter reported and range of 4.978 to 4.982 Å were reported for *c*.[7] Its structure has two hexagonal close-packed sublattices which are interpenetrating, one with aluminum atoms and other with nitrogen atoms, ideally displaced from each other along the *z*-axis by 3/8*c* as shown below in Fig.2.1a. The wurtzite AlN crystal can be regarded as stacked [AlN_4] tetrahedral units. The N and Al atoms are stacked in ABABAB sequence, which leads to a high polarity along the [001] direction.[11]

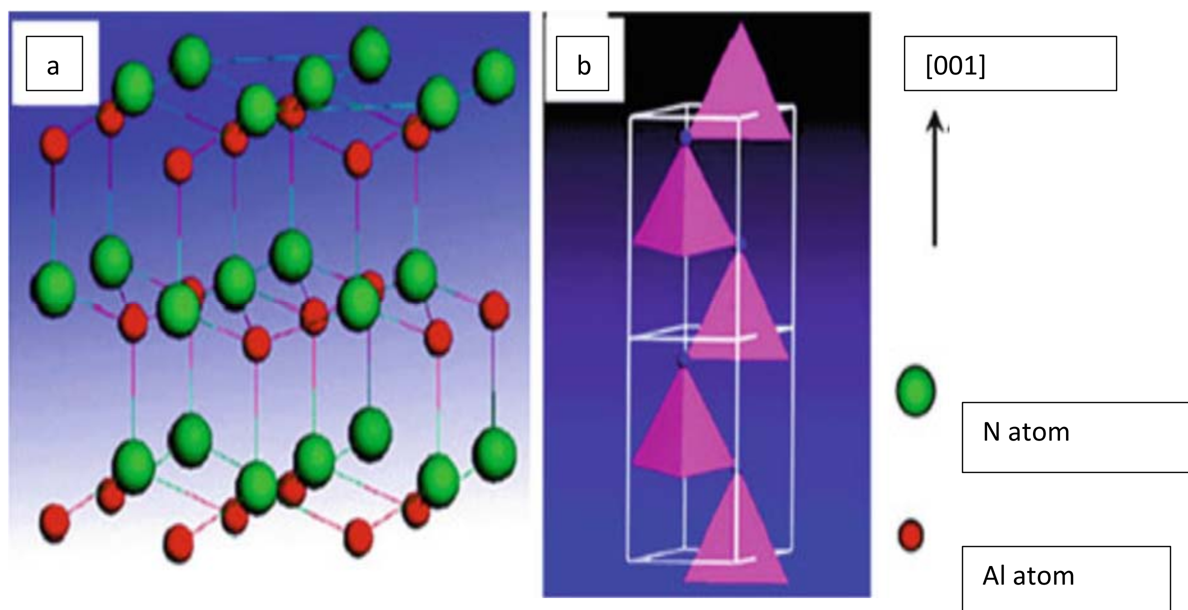

Fig. 2.1: (**a**) Hexagonal closely-packed structure of wurtzite AlN. (**b**) [AlN_4] tetrahedral units stacking along the [001] direction.[11]

2.3 Thermal and chemical properties

AlN has a melting point higher than 2000°C and it an exceptional hard ceramic material. The **thermal conductivity,** *K* of AlN at room temperature 2.85 W· cm^{-l} K^{-l}.[6,7,8] However, it varies with temperature. *Slack* and *Bartram* noted that, in term of thermal expansion, AlN is isotropic with value of 2.56 $x10^{-6}$ K^{-l} at a room temperature.[7] Its stability in inert atmospheres is very high but aluminum oxide layer is formed at above 700°C in air. This oxide layer shields the material from 700°C to around 1400°C at which total oxidation occurs.[6,7]

The chemical stability of AlN indicates its inertness to many chemical etches. A number of AlN etches have been reported in the literature, for example, wet etching which include etching in aqueous solutions, electrochemical etching in electrolytes and defect-selective

chemical etching in molten salts.[8] However, high-quality single-crystal AlN is yet to undergo these etches. Auger electron spectroscopy, X-ray and ultraviolet photoemission spectroscopy (XPS, UPS), ultraviolet photoelectron spectroscopy, and electron spectroscopy have been used to investigate the surface chemistry of the AlN. *Slack* and *McNelly* observed in one of the investigations that the AIN surface grows 50 - 100 Å thick oxide layer in a day under the atmospheric air. However, the further deterioration of the AlN samples was protected and resisted by the oxide layer.[7,8]

2.4 Electrical properties

Electrical characterization of AlN is restricted to resistivity measurements due to the low intrinsic concentration, impurity energy levels, and the deep intrinsic defect. *Kawabi et al.* carried out the resistivity measurements on single crystal AlN and got resistivity values range between p = $l0^{ll}$ -10^{13} Ω cm, a value consistent with other reports.[7]

Advancement in growth techniques has made it possible to grow crystal of improved quality which can show both n- and p-type conductions. This in turn help the efforts to measure both the electron and hole Hall mobilities. A very rough estimate of the hole mobility is found to be 14 cm^2 /Vs at 290 K by *Edwards et al*, and k*awabi* et al.[6,7,11]

2.5 Mechanical properties

Using a Knoop diamond indenter, the hardness of AlN was measured along the basal plane (0001) to be ≈ 12 GPa. Knoop hardness in other direction perpendicular to the *c*-axis has been noticed to be in range of 10 – 14 GPa. The mechanical properties of bulk AlN were carried out on single crystal. The bulk modulus B was found to be in ranges of 160 GPa to 201 GPa and Young's modulus E measured to be between 193 to 208 GPa.[3,6,7,11] The latter

was obtained by fitting the results of surface-acoustic-wave measurements made on epitaxial AlN films and by Brillouin scattering measurements made on an AlN single crystal.[7]

2.6 Optical properties

High oxygen affinity of AlN and its hard elimination have been observed by many people in different types of AlN films during optical and luminescence studies. Oxide coating is formed on the surface of each grain while some oxygen is dissolved in the AlN lattice.

Photoluminescence and cathodoluminescence characteristics of AIN were reviewed recently by *Harris* and *Youngman.* AIN doped with oxygen was found to emit a series of broad luminescence bands at the near-ultraviolet frequencies at room temperature after being irradiated with ultraviolet light. Samples being powder, single-crystal or sintered ceramic.[1] Characterization of high-quality AIN by *Yim et al*. using optical absorption to determine the room-temperature band gap is found to be 6.2 eV.[7]

The refractive index (n) measurements of amorphous, polycrystalline, and single epitaxial AlN thin films were found to be between 1.99 - 2.25 with many groups reporting n = 2.15± 0.05. Structural order affects the refractive index values. Amorphous films have value between 1.8 to 1.9, polycrystalline films between 1.9 to 2.1, single-crystal epitaxial films having highest values between 2.1 to 2.2.[3,6,7]

AlN basic properties are given in table 2.1 below.

Table 2.1 Basic properties of AlN at 300K [a]

Basic parameters:		**Remarks**
Crystal structure	Wurtzite	
Group of symmetry	C^4_{6v}-$P6_3mc$	
Number of atoms in 1 cm^3	9.58×10^{22}	
Debye temperature	1150 K	
Melting point	3273 K	
Density	3.255 g cm^{-3} 3.23 g cm^{-3}	X-ray
Dielectric constant (static)	9.14	300 K, reflectivity
	8.5	300 K
Dielectric constant	4.84 4.6 4.77	300 K, reflectivity 300 K
Refractive index	2.1 - 2.2	300 K, Epitaxial films and monocrystals
	1.9 - 2.1	300 K, Polycrystalline films
	1.8 - 1.9	300 K, Amorphous films
Electron mass (m_e)	0.4 m_o	300 K
Hole masses k_z, m_{hz} k_x, m_{hx}	3.53 m_o 10.42 m_o	300 K
hole masses (light) k_z, m_{lz} k_x, m_{lx}	3.53 m_o 0.24 m_o	300 K

Hole masses (split-off band) k_z k_x	$0.25m_o$ $3.81m_o$	300 K
mass of density of state m_v:	$7.26m_o$	300 K
Electron affinity	0.6 eV	300 K
Lattice constant, *a*	3.11(1) Å	300 K; X-ray diffraction on ultrafine powder
	3.112 Å	300 K
Lattice constant, *c*	4.98(1) Å	300 K; X-ray diffraction on ultrafine powder
	4.982 Å	300 K
	4.979 Å	300 K
Thermal diffusivity	1.47 cm^2 s^{-1}	
Thermal conductivity	2.85 W cm^{-1} $°C^{-1}$	300 K. experiment
Thermal expansion coeff, linear	$\alpha_{ort} = \alpha_c = 5.27x10^6$ $\alpha_{\|\|} = \alpha_a = 4.15 x10^{-6} K^{-1}$	T=20...800 °C. X-ray, epitaxial layers
Radiative recombination coefficient	0.4 x 10^{-10} cm^{-1} s^{-1}	300 K
Optical phonon energy	99.2 MeV	300 K

[a]Adapted from: Electronic archive: "New Semiconductor Materials. Characteristics and Properties"

2.7 Doping and luminescence of AlN with rare- earth elements

Due to the optical and luminescence properties often exhibited by rare-earth (RE) and transition-metal (TM) dopants, some important photonic and optoelectronics applications have been developed.[1,6,23] Zanata in 1998 was first to report photoluminescence of erbium doped SiN and followed shortly by Steckl to demonstrate visible emission in Erbium doped GaN. Since then rare-earth doped wide band gap (WBG) semiconductors like AlN and some insulators have been used for visible emission at room temperature. It was reported that the luminescence intensity of the rare-earth ions was improved by a wide band gap host, since that time III-V semiconductors were emerging as potential candidates for light emitting diodes. Ion implantation at low atomic concentrations or in situ doping at low percentages of the rare-earth ions was used to incorporate RE ions in crystalline hosts and it was believed that the quality of the host lattice was essential to the RE luminescence.[1] However, Zanata and Nunes observed that green room temperature luminescence from an Erbium-doped silicon nitride film deposited by reactive sputtering in nitrogen. The silicon nitride film was an amorphous and it gave visible emission and it was estimated to be 10 atomic percentage dopant concentrations. Zanata and Steckl groups discovered of amorphous and crystalline luminescence in rare-earth doped wide band gap semiconductor started the (endured) striving of achieving practical visible light emission devices .[1,6]

Luminescence spectroscopy is a valuable instrument to explain the electronic structure of complicated localized centers and the processes of energy transfer among different centers in the materials.

When these rare-earth doped III-V nitride materials are excited by various means of excitation, most trivalent rare-earth (lanthanoid) ions of Ce^{3+} - Yb^{3+} produce efficient luminescence of line spectra owing to the $4f^{n*} \rightarrow 4f^{n}$ transition in the visible to near-infrared region. Trivalent rare-earth ions of Ce^{3+} - Yb^{3+} have the electron configuration $4f^{n}5s^{2}5p^{6}$(n = 1-13). The configuration of divalent ions includes one more 4*f* electron. The 4*f* electron shell is located inside the *5s5p* shell, so the influence of the crystal field on the 4*f* energy levels is weak, much weaker than on the *3d* levels. As a result, the 4*f* levels in solids are not very different from those of the free ion state, and further do not change very much when the host lattice is changed. Absorption and emission spectra of trivalent rare-earth ions owing to 4f $\rightarrow$ 4f transitions are thus composed of a number of lines. According to the configuration- coordinate model, it is considered that an electron always occupies a stationary energy state corresponding to each position of nuclei, and that the latter are vibrating within the potential determined by the electron due to the fact that electrons move 10^{3} or more faster than nuclei. The extent of 4*f* wavefunctions does not change very much by excitation.[10]

Information that could deduced from luminescence spectra are;

Excitons

Excitons are localized excited electronic states in a nonmetallic crystalline lattice. The materials with an appreciable degree of covalent bonding as occurred in III-nitride semiconductors exhibit Wannier-Mott exciton model. The electron-hole pair with a minute binding energy can be regarded as interacting due to the extension of excitation energy over several unit cells. Excitons may form complexes by a bond to defects as donors,

acceptors or dislocations.[10,21] In this case, ionization energy of the defect approximately increasing linearly with binding energy with lowered exciton transition energy.[15]

Donor- acceptor pairs

"The existence of pairs of oppositely charged defects in semiconductors provides efficient radiative recombination centers for excitons.[21] While the ground state of the system is given by the ionized donor and acceptor with interim purity distance *R,* photo-excitation leads to a neutral pair in an excited state. This state can be described as an exciton bound to the ionized donor-acceptor core or as a neutral donor and a neutral acceptor perturbed by the interaction with each other.[10] A simple approach based on the effective mass theory leads to the recombination transition energy."[10]

$$hv= E_g-(E_D + E_A)+ e^2/\varepsilon R$$

E_A and E_D being the ionization energy of the donor and acceptor respectively, ε is dielectric

Deep level centers

Deep level centers often form localized states in the fundamental band gap of semiconductors. They originate from intrinsic defects (vacancies, anti-sites, dislocations), impurities (substitutional, interstitial) or complex structures (combinations). "Deep level centers in low concentration compete very often with numerous other defects in the crystals. [21, 25] The most prominent deep level luminescence centers are rare earth ions (f-elements) and transition metals (d-elements) in solids when the concentration is so low that the centers do not interact with each other.[25]" The electronic states originate from excited levels of the partially unfilled inner shell of 4*f*-orbital of Rare-earth elements can be

described by both the quantum mechanical theory of free ions and by the basic approach of crystal field theory.[12,27]

“Energy transfer phenomena are concerned with the general question of how the energy which initially is localized at an excited center, called an 'energy donor', is transferred to another center, labeled an 'energy acceptor.’ The parameters determining an energy transfer are the distance (and thus the concentration) of the involved centers, the kind and coupling strength of their mutual interaction and their energy matches. Energy transfer processes lead to a temperature and concentration dependence of the radiative transition intensities of (energy-) donor and acceptor centers and can thus also account for quenching phenomena.[6,27]”

2.8 RF magnetron sputtering

The deposition of thin films by sputtering is one of resourceful techniques to produce high quality films. It is process that provides films with greater adhesion and homogeneity, better-controlled composition, and allows good control of film thickness. Radio frequency (RF) sputtering is an example of sputtering method (PVD) process that uses radio frequency excitation to cause gas molecules to collide with a target, moving the target material by the mechanical impact of the sputtering gas.[1] Enhanced sputter method which is well known and used for many industrial applications because it favors the possibility of getting high quality films at low and high substrate temperatures and low operating pressure with higher deposition rate.[5,6] The process is used to make thin film, especially when using non-conductive materials. In this process, a thin film is grown on a substrate placed in a vacuum chamber.

"Sputter uses a close magnetic field to trap electrons and allow plasma to be generated at low pressure. It starts when a negative charge is applied to the target material causing a plasma or glow discharge. Positively charged gas ions generated in the plasma region are attracted to the negatively biased target plate at a very high speed. This collision creates momentum transfer and ejects atomic size particles from the target. These particles are deposited on the substrate in the form of a thin film with the help of the powerful magnet."

The binding energy of the atom to the substrate determined the motion of the atom diffusion, which in turn influenced by nature and temperature of the substrate.[1] For simple compounds, the stoichiometric product is often the most likely compound to be deposited, because there are few alternative compositions and structures. The purity of the initial elements or components determines the composition of the deposited film.[1]

The properties of the deposit can be seriously affected by the conditions used for sputtering. There are numerous parameters that control the deposit, such as; magnetic field effects, the plasma, the quantity of reactive gas, the gas flow, the pressure in the deposition chamber, the energy parameters and the sputtering current and bias voltage. Figure 2.2 below shows the schematic diagram of RF magnetron sputtering system.

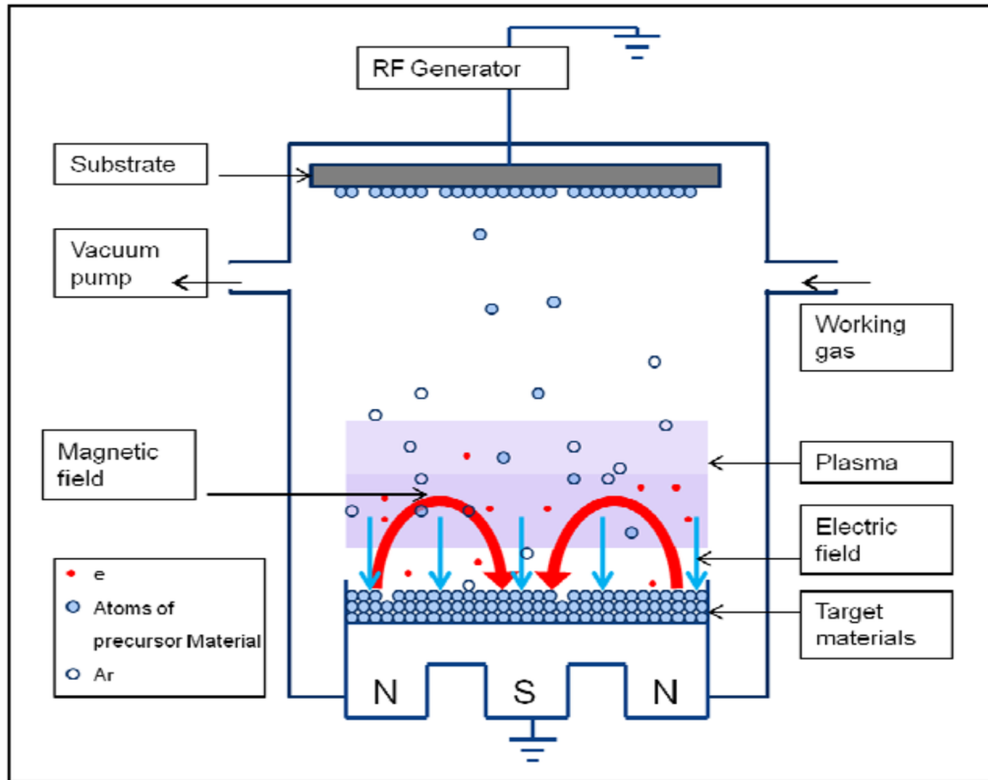

Fig. 2.2: Schematic Diagram of RF Magnetron sputtering system [37]

Chapter 3: EXPERIMENTAL SET-UP AND TECHNIQUES

3.1 Films growth and substrate temperature

The basic work in this study is the growth of films. Reactive magnetron sputtering system was used to grow all the films in a deposition chamber of an ultra-high vacuum. Nitrogen gas was used as sputtering gas instead of Argon. Silicon (100) and Silicon (111) were used as substrates for all the depositions. Substrates were cleaned using methanol and air cleaner.

Specially designed substrate holders were used to deposit films at different temperatures. These special holders exhibit holes for keeping liquid nitrogen to be in contact with substrate in order to keep substrate at very low temperature for low temperature deposition. The holes in holders are cylindrical in shape and of dimension 25 cm long by 1 cm diameter. The growth temperature ranged from -196°C to 700°C. The deposition process was performed under ultra-vacuum condition using a turbo pump and cryogenic pump. RF guns were used to deposit films. The inside of the chamber contain crystal thickness monitors to monitor the film thickness during growth. Films deposited total thickness was ranged from 300 nm to 450 nm. Cryogenic pump and growth chamber temperatures were kept down using water pump after the film deposition.

The investigated films in this study were doped films grown by co-sputtering aluminum and rare-earth element simultaneously. A small piece of Rare-earth element was placed inside the main host (Al). The growth rate for these films was controlled by the radio frequency power.

Fig.3.1: RF magnetron sputtering system used in the film deposition

3.2 Characterization techniques

3.2.1 X-ray diffraction (XRD)

The process by which electromagnetic radiation with a few angstroms, without changing its wavelength, is converted through interference by the lattice to a vast number of observable "reflections" with characteristic directions in space is called *X-ray diffraction.*

The structural characterization was carried out by recording the x-ray diffraction (XRD) pattern of the samples. XRD pattern was performed using a Rigaku miniflex2 x-ray diffractometer with Cu/30 kV/15 mA radiation (λ=1.5418 Å) see figure 3.2. Theta- 2theta (θ - 2θ) scans were taken using the diffractometer that is equipped with miniflex2 goniometer and counter. X-ray from copper with voltage of 30 kV and 15 mA was used for illumination

purpose. The scanning range was from 20° – 80° at 2.00 degree/minute. The crystal structures of films were determined by the presence of the Bragg diffraction peaks in XRD spectrum. Experimentally obtained diffraction patterns of the samples were compared with the standard powder diffraction files published by the inorganic crystal structure database (ICSD).[5]

The average crystallite size of the film can be calculated using the Scherer's equation below:[9]

$$t = (0.9\lambda)/\beta\cos\theta \qquad (2.1)$$

Where, β is the full width at half maximum intensity in radians, λ is the wavelength of the x-ray. The parameters *a* and *c* for crystallographic systems in the present study are calculated from the following equation using the (hkl) parameters and the interplanar spacing d for hexagonal crystal,

$$\frac{1}{d^2} = \frac{4}{3}\{\frac{h^2+hk+l^2}{a}\} + \frac{l}{c^2}^2 \qquad (2.2)$$

Grain size and lattice strain from XRD data

Among the available methods to estimate the crystallite size and lattice strain are the Scherrer's equation, Williamson and Hall analysis and Warren-Averbach analysis.

Scherrer's equation is used for the estimation of the crystallite size in the form of powder which is limited to nano-scale particles and provides a lower bound on the crystallite size.

Williamson and Hall (W-H) analysis is used to study the individual contributions of crystallite sizes and lattice strain on the peak broadening.

Warren-Averbach method employs the deconvolution Fourier-transform (stokes method) for the determination of the intrinsic physical line profile, followed by the Fourier method for evaluation of lattice imperfections.

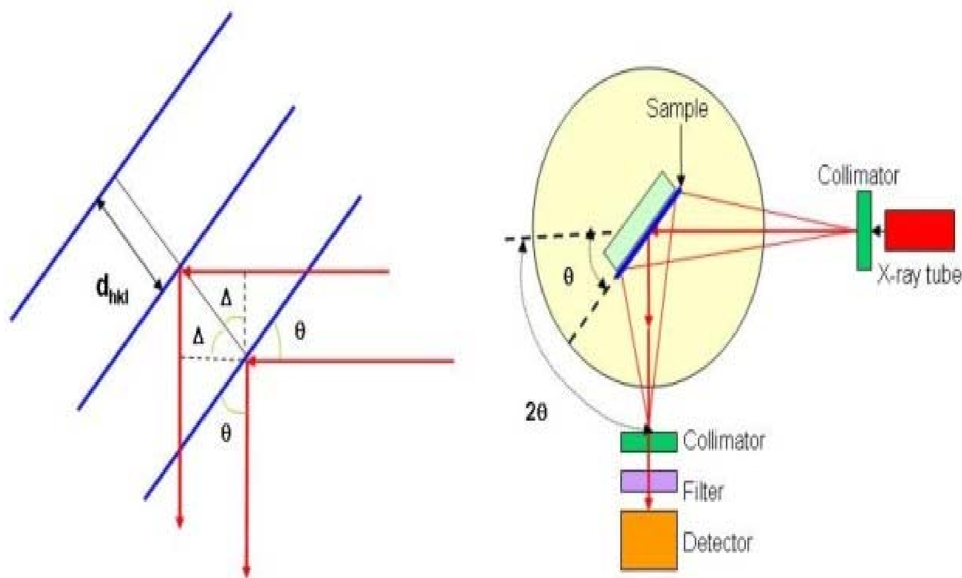

Fig. 3.2: Schematic diagram of the XRD basics[13]

3.2.2 Scanning electron microscopy (SEM)

Scanning electron microscope (SEM) is a versatile tool used in material characterization. It is used for surface morphology, topography and elemental mapping. Scanning electron microscope (SEM) images the sample surface by scanning it with a high-energy beam of electrons in a raster scan pattern. The electrons interact with the atoms that make up the sample producing signals which contain information about the sample's surface topography, morphology as well as particle size and shape.

The morphology and structure of the films were examined by Quanta 200 Scanning electron microscope. Figure 3.3 below shows the SEM/EDX device used in this study.

3.2.3 Energy dispersive X-ray (EDAX) analysis

EDAX is a widely used technique for identifying the elemental composition of the specimens, on an area of interest thereof under the SEM. The EDAX analysis works as an integrated feature of a scanning electron microscope (SEM). "During EDAX analysis, the specimen is bombarded with an electron beam inside the scanning electron microscope. The bombarding electrons collide with the specimen atom's own electrons, knocking some of them off in the process. A position vacated by an ejected inner shell electron is eventually occupied by a higher-energy electron from an outer shell. To be able to do so, the higher-energy electron must give up some of its energy by emitting an x-ray, which is unique for each element."[30] The EDAX tool used in this study is an integrated part of Quanta 200 SEM. The parameters of EDAX tool used are stated below:

Parameter	**Value**
Primary energy	30 keV
Tilt angle	0°
Take off angle	35°
Azimut angle	29.5^{o}
Real time	200000 ms
Life time	187188 ms
Detector type	XFlash 5010
Si dead layer	0.029 µm
Detector thickness	0.45 mm
Window type	Slew AP3.3
Fane factor	0.112
Mn FWHM	130.5298 eV
Calibration, line	4.998 eV
Calibration, abs	-477.559 eV
Channels	4096

Table 3.1: EDAX parameters used in the study

Fig. 3.3: Quanta 200 SEM/EDX used in the study

3.2.4 Atomic force microscopy (AFM)

Atomic force microscopy (AFM) is a “specific type of microscopy that uses the basic principle of scanning a surface with a very sharp tip to image and measure properties of material surfaces. The AFM provides a 3D profile on a nanoscale, by measuring forces between a sharp probe (radius less than 10nm) and surface at very short distance (0.2 – 10nm probe-sample separation). The probe is supported on a flexible cantilever and the AFM tip gently touches the surface and records the small force between the probe and the surface. This force can be described using Hooke’s law:[34]

$$F = - k.x \qquad (3)$$

Where F = force; k = spring constant; x = Cantilever deflection.”

AFM measurements enable the characterization of films morphology evolution. In particular, analysis of the films surface roughening and grain coarsening processes. The dimension of each film scanned in the study is 5µm X 5µm. “Roughness data were obtained directly from the images by AFM software whereas the typical surface grain size was obtained by averaging the different values found in the images.[17]” Figure 3.4 below shows the image of the AFM chamber used in the study.

Fig. 3.4: Atomic force microscope used in the study

3.2.5 Fourier Transform infrared (FTIR) spectroscopy

FTIR spectroscopy is a technique that provides information about the chemical bonding or molecular structure of materials, whether organic or inorganic. It may also be used to identify unknown elements present in a specimen. “The technique works based on the fact

that bonds and groups of bonds vibrate at characteristic frequencies. A molecule that is exposed to infrared rays absorbs infrared energy at frequencies which are characteristic of that molecule. During FTIR analysis, a spot on the specimen is subjected to a modulated IR beam. The specimen's transmittance and reflectance of the infrared rays at different frequencies is translated into an IR absorption plot consisting of reverse peaks. The resulting FTIR spectral pattern is then analyzed and matched with known signatures of identified materials in the FTIR library.[27]" FTIR of the films were studied to observe the likely subsurface bonds formation of other than the doped AlN on the surface. The operation of the tool is in transmittance mode and the wavenumber range was from 300 - 2200 cm^{-1}, Figure 3.5 shows a typical FTIR graph of AlN powder and thin film.

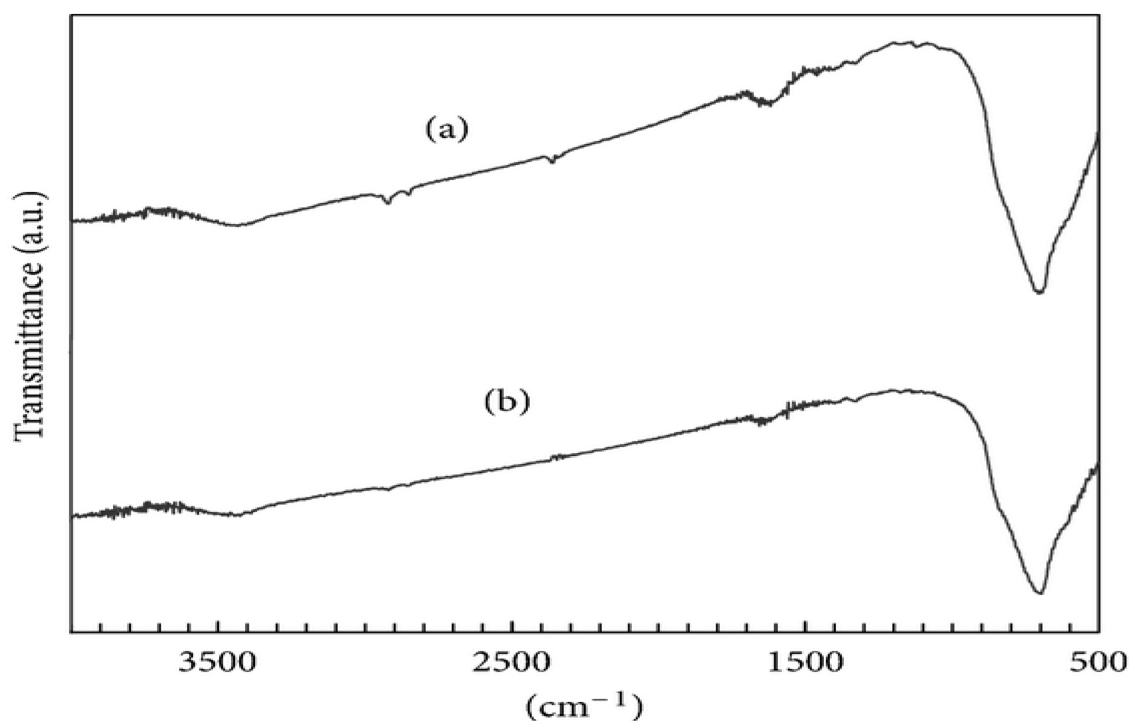

Fig. 3.5: Transmission FTIR spectra: (a) The original AlN powder before electrophoretic deposition; (b) The AlN film scraped from the Al cathode.[32]

3.2.6 Thermo-gravimetric Analysis (TGA)

Thermo-gravimetric Analysis is an analytical technique used to determine a material thermal stability, in which the mass change of the sample is recorded continuously as a function of temperature, as it is heated or cooled at a controller rate. Both quantitative and qualitative information could be obtained from thermogram which is a plot of mass as a function of temperature. Changes in the mass of the sample occurs as a result of breaking and/or formation of various physical and chemical bonds at elevated temperature that lead to the evolution of volatile products or formation of reaction products. Thus TGA curve provides information regarding the thermodynamics and kinetics of various chemical reactions, reaction mechanisms, and intermediate and final reaction products.[27] The films were subjected to heating range from 30°C – 900°C to study their thermal stabilities. Typical thermogram graphs for AlN samples with or without phosphate species are shown below:

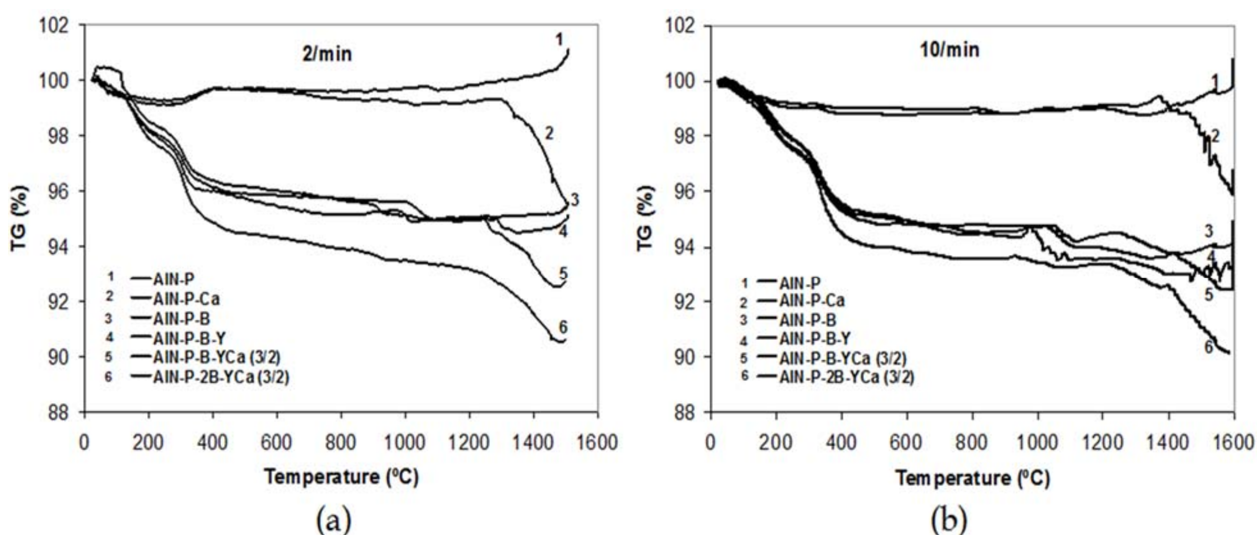

Fig. 3.6: Thermogravimetric curves of the AlN samples without or with phosphates species with different added amounts of sintering aids and organic specimens: (a) obtained at a heating rate of 2°C/min; (b) obtained at a heating rate of 10°C/min.[33]

3.2.7 Photoluminescence

Luminescence in solids is the phenomenon in which electronic states of solids are excited by some energy from an external source and the excitation energy is released as light. When the energy comes from short wavelength light and results in the emission of higher wavelength with lower energy, the phenomenon is called photoluminescence (PL). Photoluminescence is divided into intrinsic and extrinsic luminescence. Intrinsic is three types, band to band, exciton and cross – luminescences. While extrinsic is divided into unlocalized and localized types.[25] Luminescence caused by intentionally incorporated impurities, like rare-earth impurities or defects is referred to as extrinsic luminescence. Intentionally incorporated impurities are activators and materials made luminescent in this way are called phosphors. Luminescence of the films was studied by using Maple II PL equipment. The GL532 nm laser with 125mW power and exit width slit 0.25mm was used as excitation source and resulting luminescence was collected by using gated CCD. Figure 3.7 shows a picture of the luminescence tool used in the study, which was recently acquired and installed by the Materials Science and Technology program.

Fig. 3.7: Maple II Photoluminescence tool used in this study

3.2.7.1 CIE color coordinate

Color characterization of a spectral distribution is done to gauge the quality of its chromaticity. This is accomplished using color coordinates. In 1931, the Commission Internationale de l'Eclairage (CIE) established an international standard for quantifying color known as CIE color coordinates. The chromaticity coordinates map all the visible colors with respect to hue and saturation on a two dimensional chromaticity diagram. The CIE coordinates are obtained from the three CIE tristimulus values, X, Y and Z.[21,27]

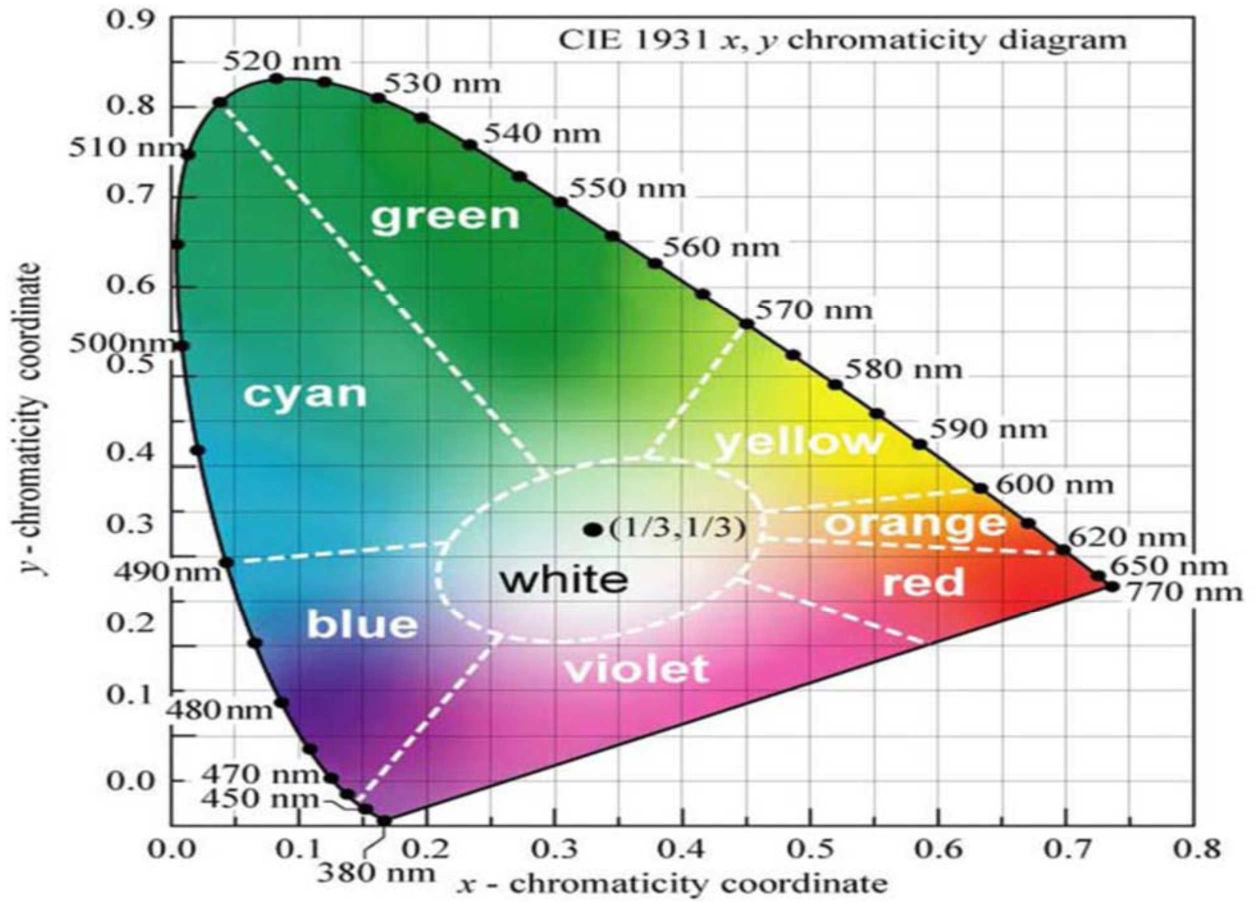

Fig. 3.8: The CIE chromaticity diagram

Chapter 4

Results and Discussion

4.1 Structural Characterization

The thin film samples used in the study were Samarium-doped Aluminum nitride (AlN) deposited at -196°C (Sm/-196), Gadolinium-doped AlN films deposited at 250°C and 450°C (Gd/250 and Gd/450), and Holmium-doped AlN deposited at 700oC (Ho/700) as shown in table below:

Sample	**Substrate temperature (°C)**	**Dopant**
Sm/-196	-196	Sm
Gd/250	250	Gd
Gd/450	450	Gd
Ho/700	700	Ho

Table 4.1: Doped AlN samples used in this study

4.1.1 X-ray diffraction

The Rigaku diffractometer with Miniflex2 goniometer operated at 30kV and 15mA was used for XRD analysis to study the structure of all films. 2theta (2θ) scans were taken from 20 degree to 80 degree. X-rays with wavelength 0.154nm from copper crystal were used for illumination purpose. The scanning was carried out from 20° – 80° with the scan speed of 2.00 degree/minute and step size of 0.020 degree. The presence of Bragg diffraction peaks in the XRD spectrum was used to analyze the crystal structure. Figure 4.1a shows XRD pattern of the doped AlN films deposited at -196°C. It can be seen from Fig. 1a that due to the absence of other peaks apart from Si (100) peak. Figures 4.1b, 4.1c and 4.1d show XRD

patterns of the doped AlN films deposited at 250°C, 450°C and 700°C respectively. As can be seen from the patterns that these exhibit crystalline structure, which is obvious from the extra peaks observed at 37.8°, 38.1° and 35.92° respectively. Diffraction peaks from Silicon substrate are also shown for Si (100) or Si (111) peaks. Those peaks appear from doped AlN indicating that, films deposited at 250°C or higher are crystalline. Absence of additional peaks from the films deposited at liquid nitrogen temperature apart from silicon peaks, confirming that they are amorphous structures.

Crystallite size (t) was calculated for all the crystalline films from the information obtained by XRD data using Scherrer's formula:

$$t = \frac{0.9\lambda}{\beta \cos\theta} \tag{4.1}$$

Where λ is the XRD wave length (0.543nm), β is the peak full width at half maximum, and θ is the Bragg's diffraction angle. According to the calculations, the average crystallite size of the doped AlN films deposited at 250°C, 450°C and 700°C are 6nm, 9nm, and 11nm respectively.

The films deposited at 250°C and 450°C are poor qualities crystalline films having low intensities and AlN (101) planes (2θ ≈ 38°).[14,15] Films deposited at 700°C (2θ ≈36o) are good qualities and have high degree of c-axis alignments, which can be confirmed by its (002) diffraction indicates a preferred orientation of AlN(001) basal plane.[14,15] The lattice constant, c was calculated from this formula; Hexagonal: $\frac{1}{d^2} = \frac{4}{3}\{\frac{h^2+hk+l^2}{a}\} + \frac{l}{c^2}^2$ for films deposited at 700°C is found to be 4.89Å {data from XRD: d = 2.498Å, (002), c = 1.6a} which is close to the literature value of 4.98 Å at 300K for the bulk AlN.

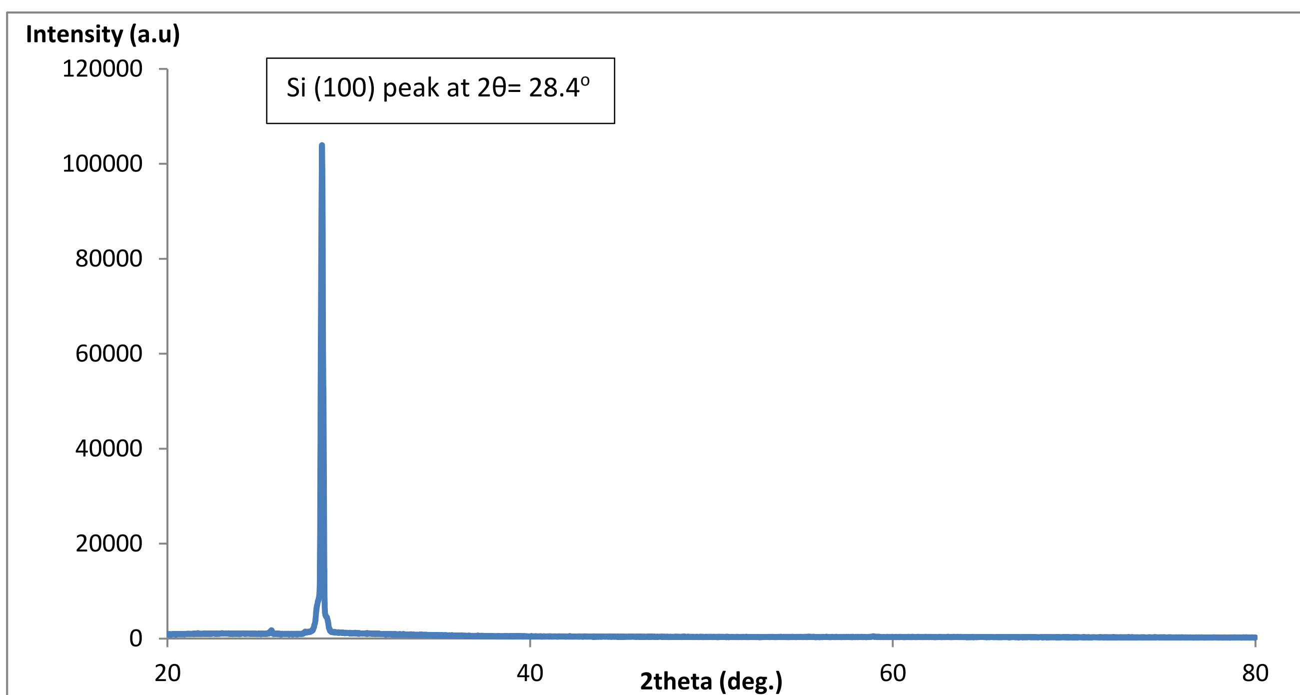

Figure 4.1a: XRD spectrum of sample Sm/-196

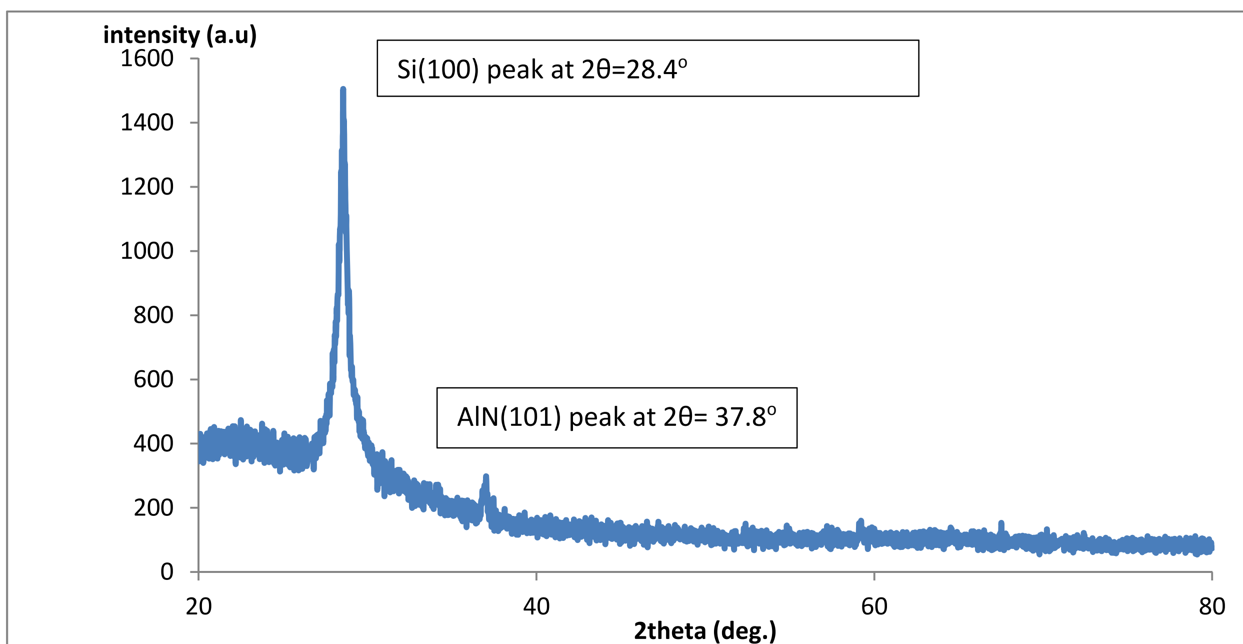

Figure 4.1b: XRD spectrum of sample Gd/250

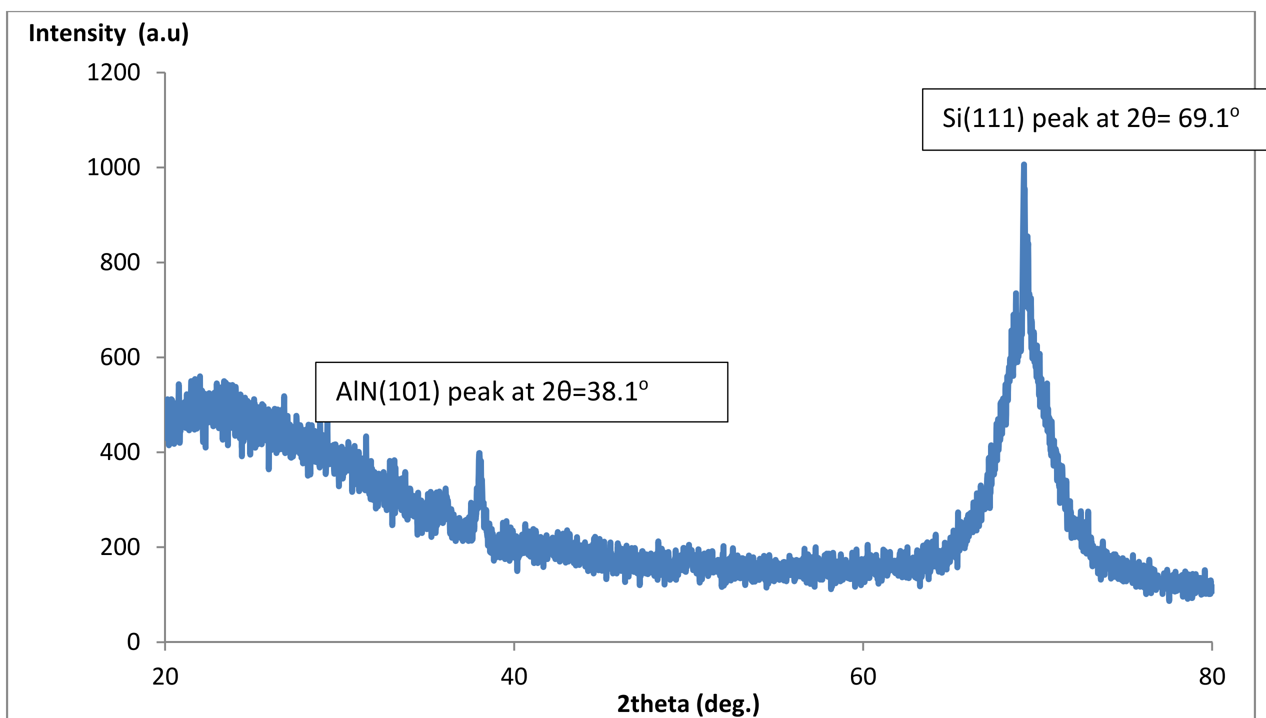

Figure 4.1c: XRD spectrum of sample Gd/450

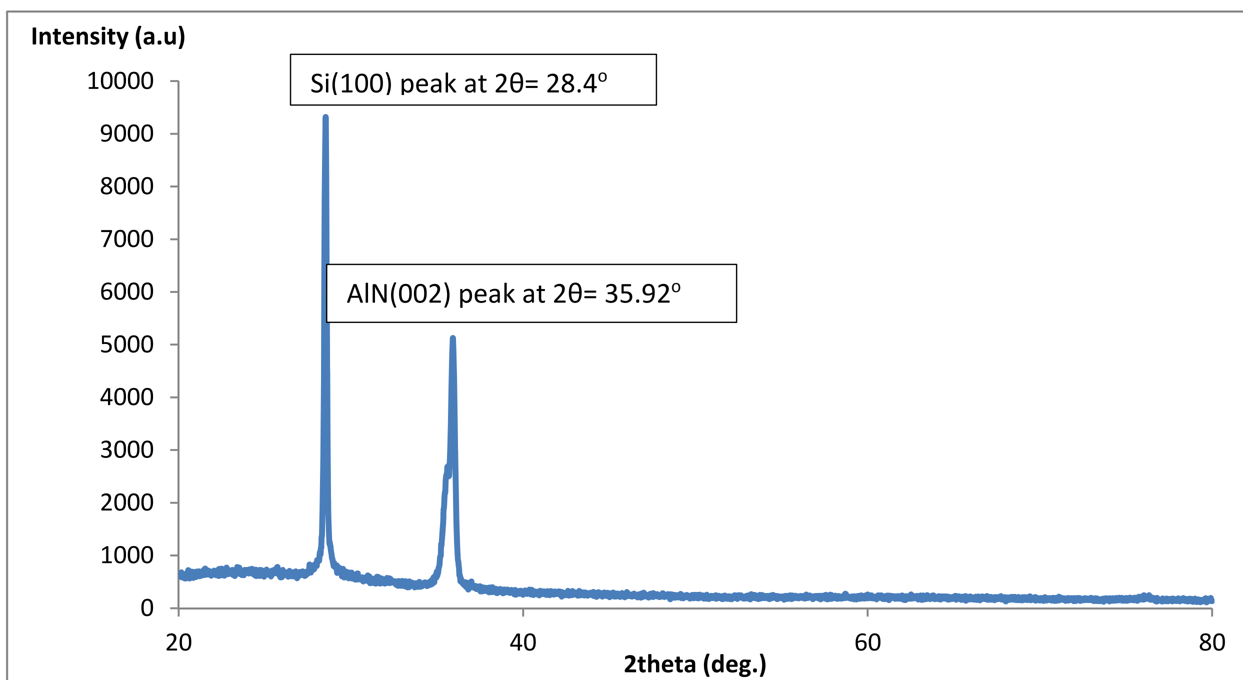

Figure 4.1d: XRD spectrum of sample Ho/700

4.1.2 Scanning electron microscopy/Energy Dispersive X-ray

The samples surfaces were scanned with a high-energy beam of electrons in a raster can pattern for structural, surface morphology and chemical compositional analysis using scanning electron microscope coupled with Energy dispersive X-ray tool (SEM Quanta 200). The top surfaces of the doped films, Figures 4.2a, 4.3a, 4.4a, and 4.5a, show that the films deposited at -196°C (Fig. 4.2a) is without long order orientation that is amorphous and the others deposited at high temperature of 250°C, 450°C and 700°C (Figs. 4.3a,4.4a and 4.5a) are crystalline with long orderliness orientations. This is in agreement with the XRD results obtained. The SEM image of sample Gd/450 shows that there is presence of dirt/impurity at the center which probable due to failure to clean the sample surface before microscopy. The average diameter of the crystallites estimated from the SEM results below are as follows; 13 nm for the film deposited at 250°C, 22 nm for the film deposited at 450°C and 27 nm for the film deposited at 700°C. The crystallites are closely packed together without any trapped pin-holes on the surface.

In the compositional analysis, the EDX spectral in the Figs 4.2b, 4.3b, 4.4b and 4.5b below, are plots of how frequently X-ray is received for each energy level. The spectral display peaks corresponding to the energy levels for which the most X-rays had been received. This measurement shows the occurrence of AlN films on the silicon substrates with the presence of very small percentage of one of doped rare-elements (Sm, Gd, Tm or Ho) and about one-tenth of the oxygen impurity.

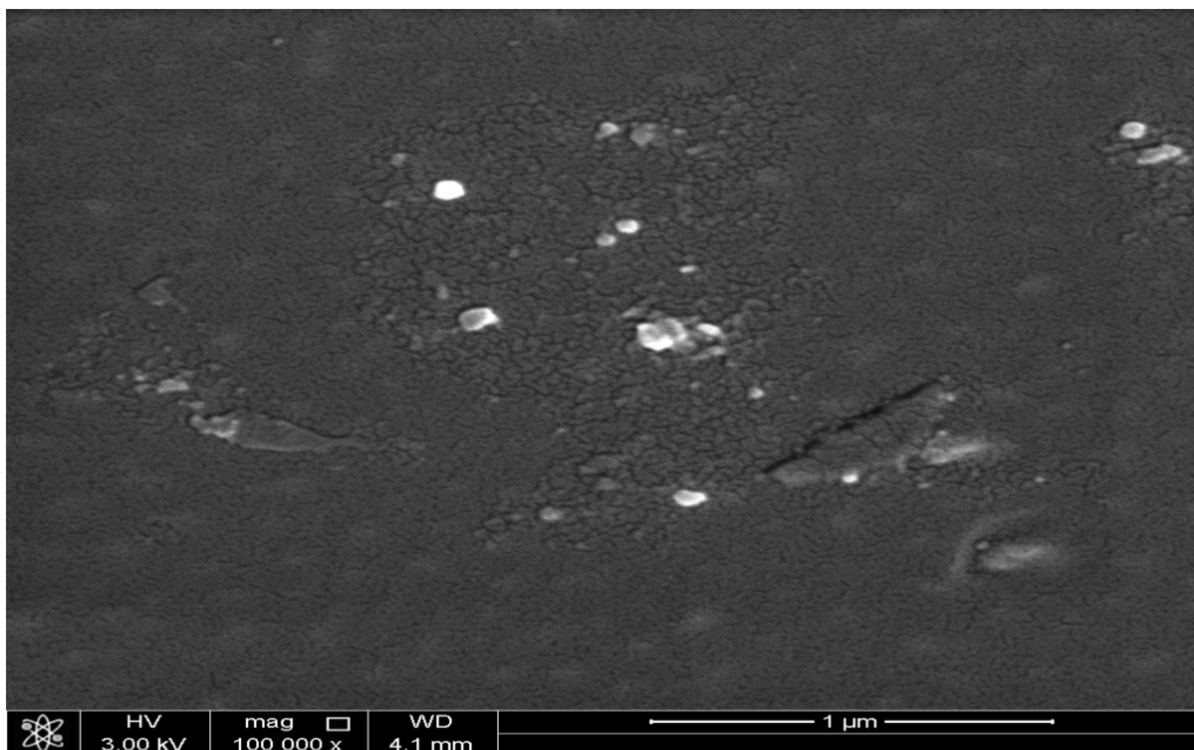

Fig. 4.2a: SEM micrograph of sample Sm/-196

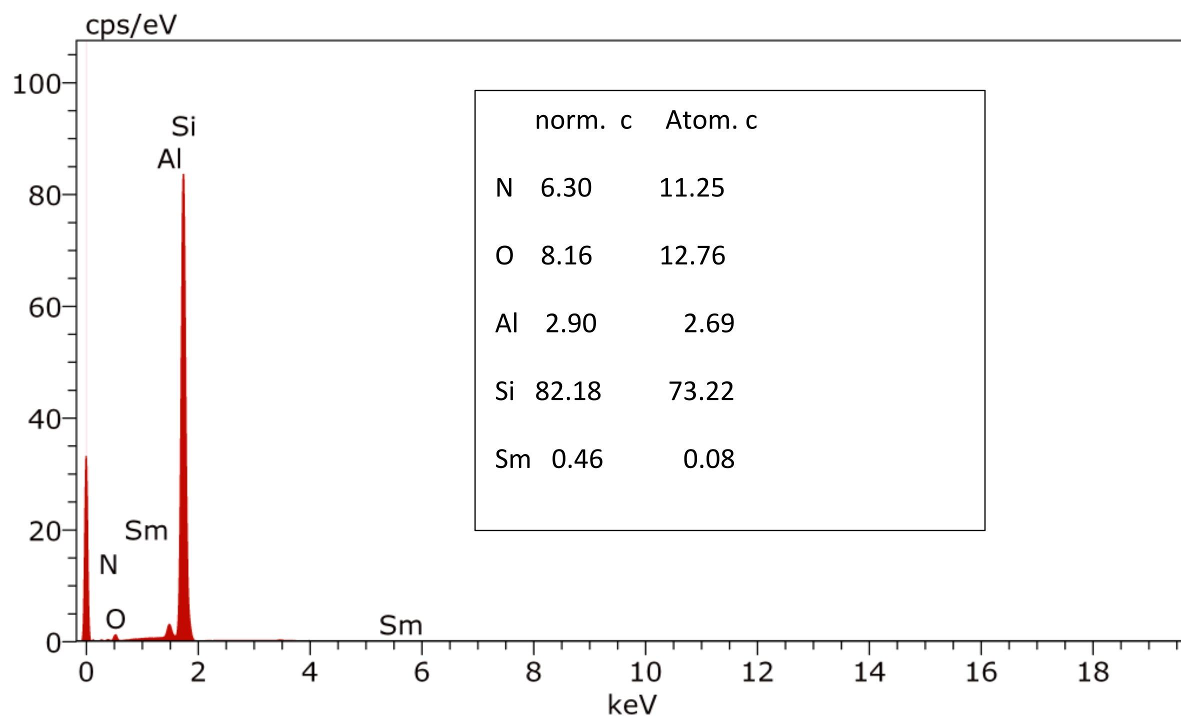

Fig.4.2b: EDX spectrum of sample Sm/-196

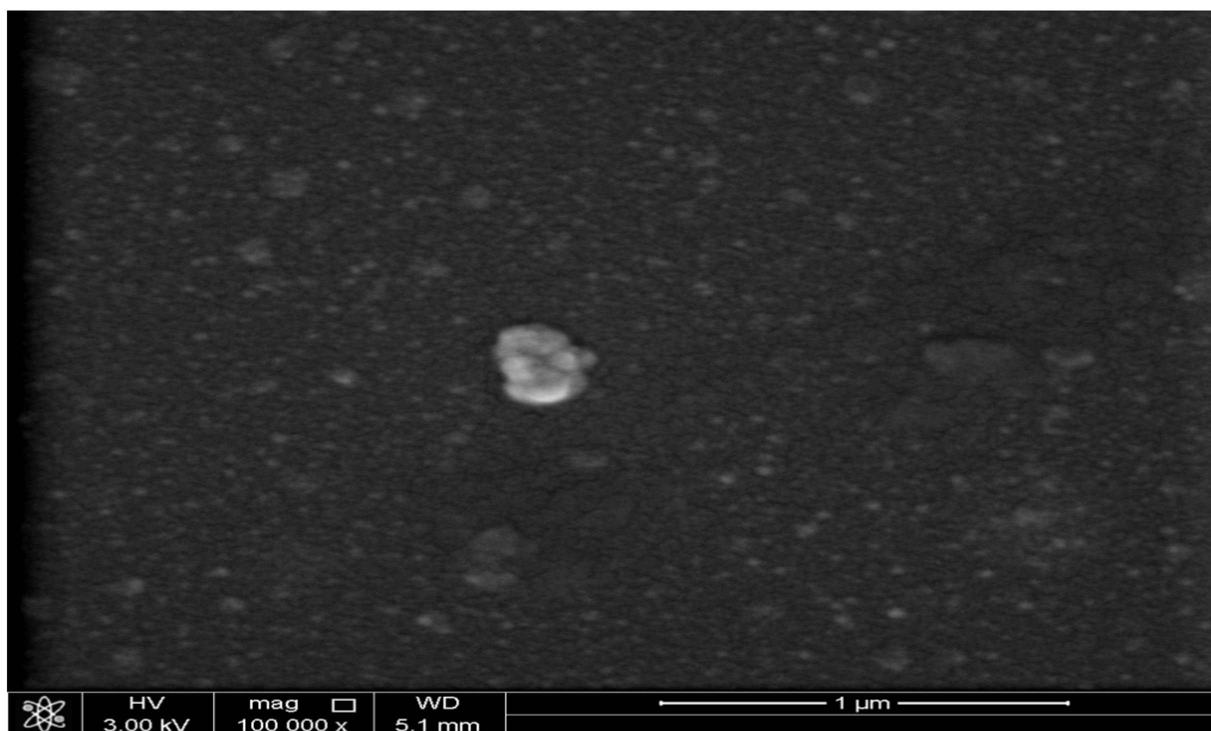

Fig. 4.3a: SEM micrograph of sample Gd/250

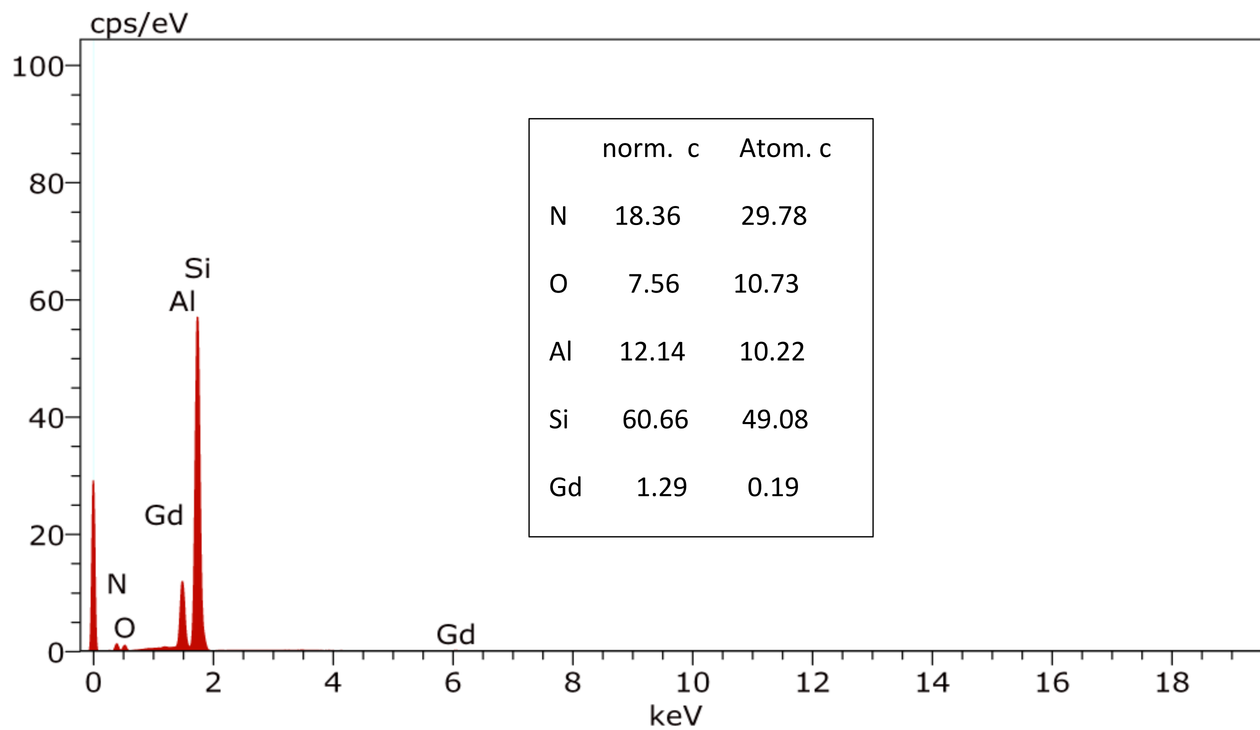

Fig. 4.3b: EDX spectrum of sample Gd/250

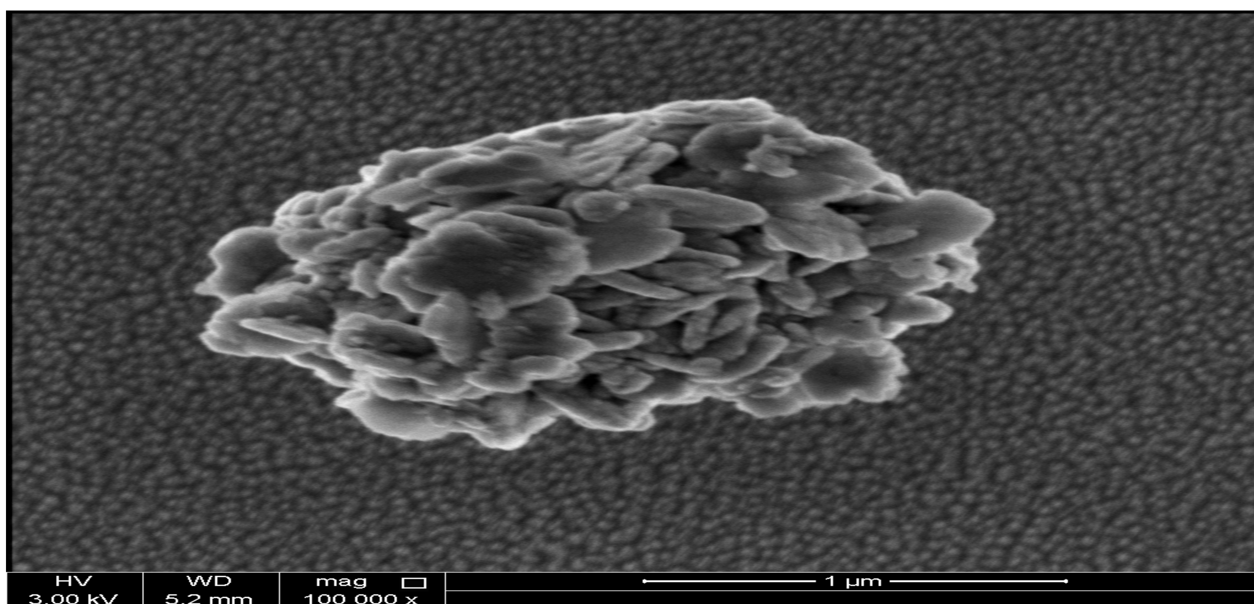

Fig. 4.4a: SEM micrograph of sample Gd/450

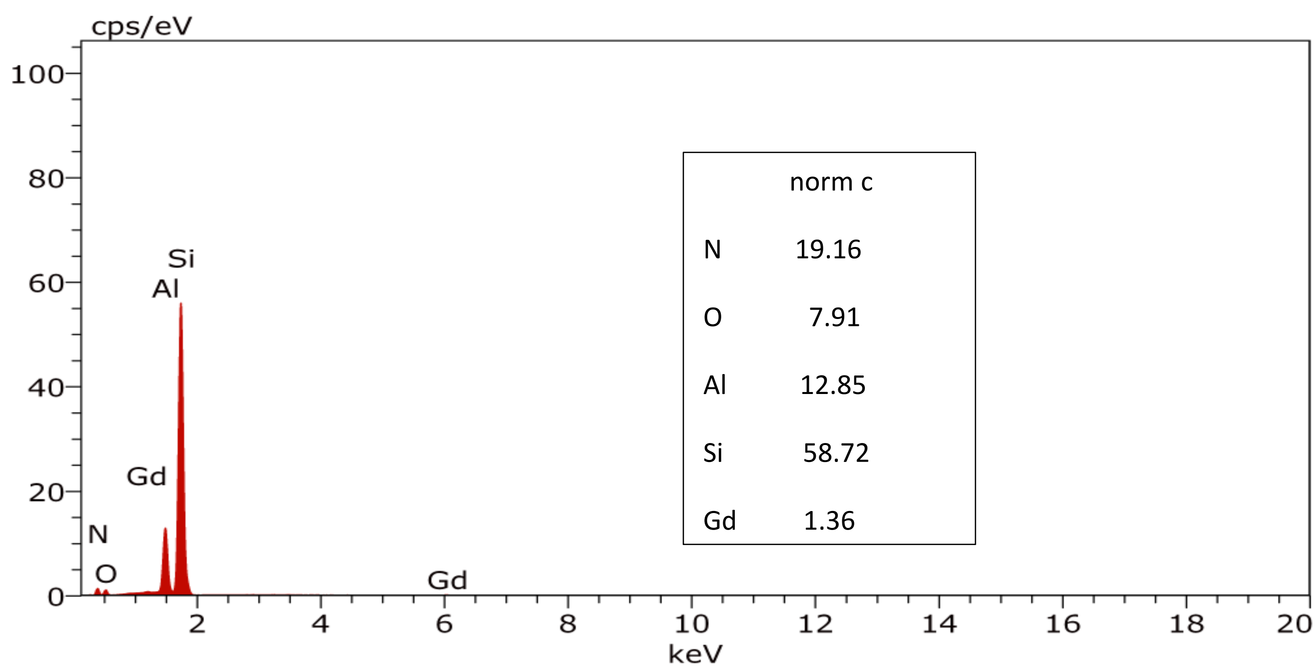

Fig.4.4b: EDX spectrum of sample Gd/450

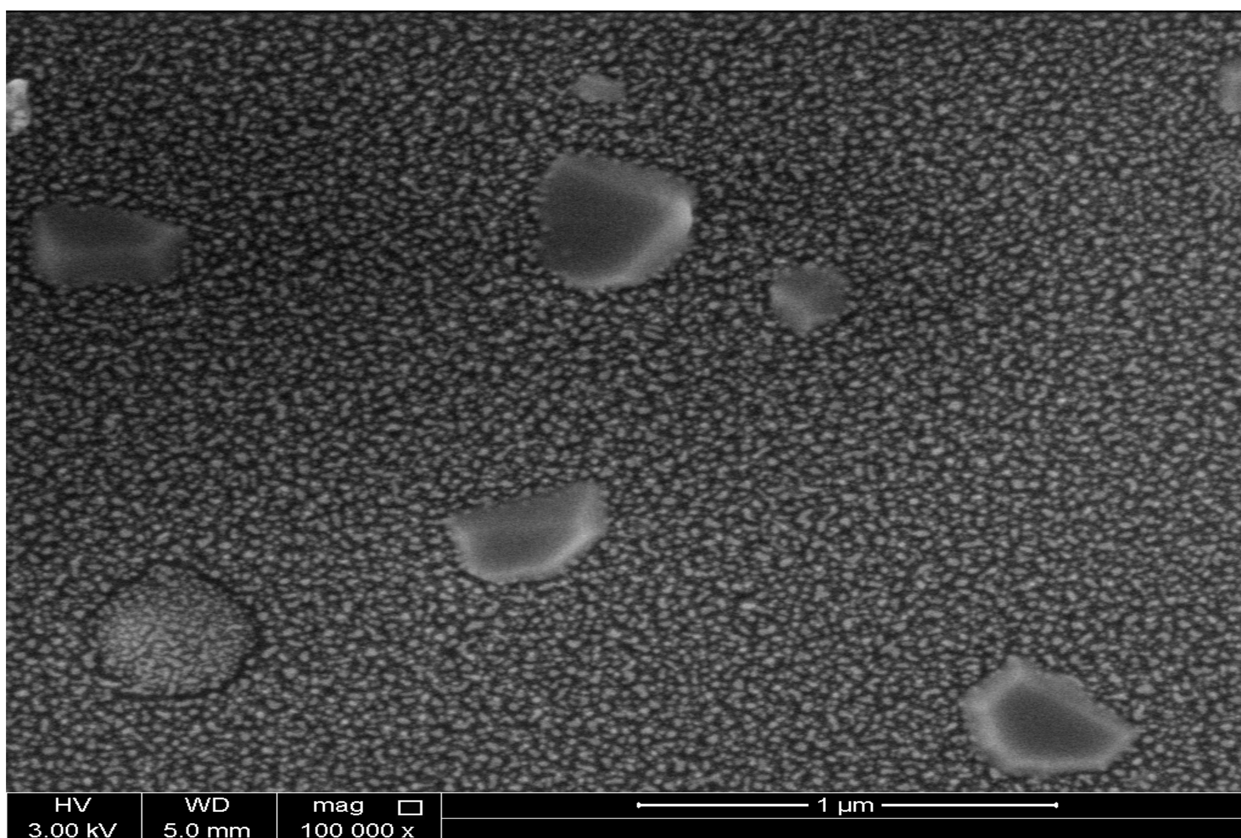

Fig.4.5a: SEM micrograph of sample Ho/700

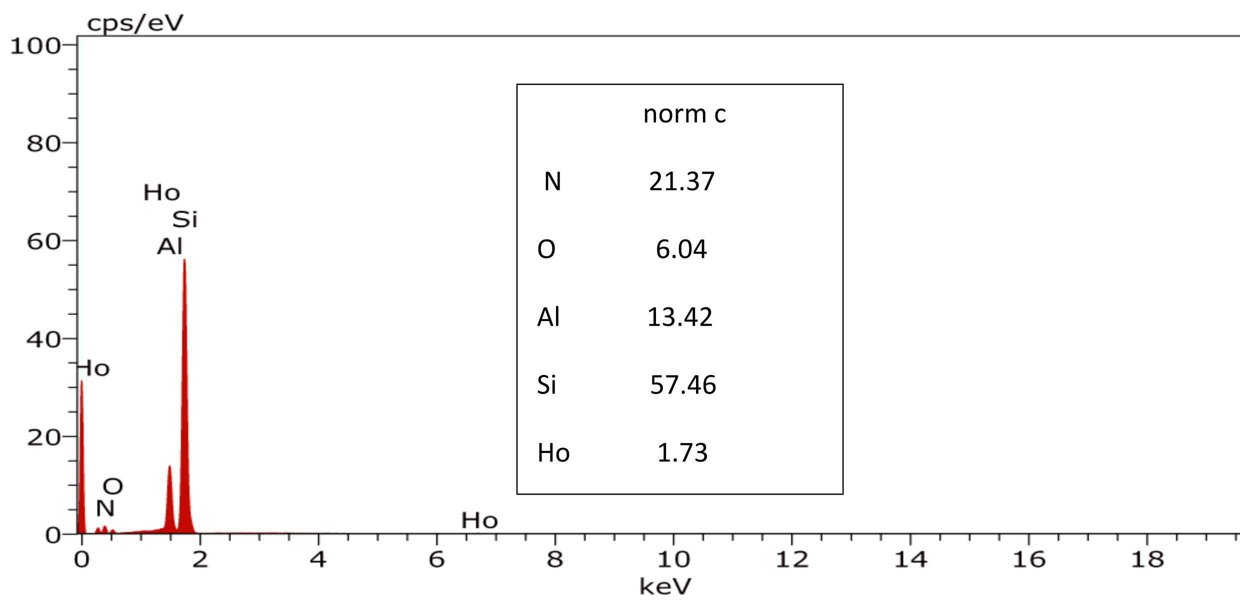

Fig.4.5b: EDX spectrum of sample Ho/700

4.1.3 Atomic force microscopy

The morphology of the deposited doped AlN layer was examined by AFM. The AFM measurement enables to characterize the films morphology evolution and in particular, “we can analyze the films surface roughening and grain coarsening processes. Roughness data were obtained directly from the images by the AFM software, whereas the typical surface grain size was obtained by averaging the different values found in the images.[17]”

In Figs. 4.6, 4.7 4.8 and 4.9 below; the doped AlN films surface morphology measured by AFM in tapping mode with AC imaging mode, for the different deposition substrate temperatures, namely; -196°C, 250°C, 450°C and 700°C. A disorder shapeless surface morphology is observed for the film deposited at -196°C while granular morphology is observed for those deposited at high temperature. Since all images are displayed in the same vertical scale, the surface roughening and grain coarsening are clearly observed.

Using image processing software, the surface roughness of the films is tabulated below:

Sample	**Surface roughness (nm)**
Sm/-196	3.799
Gd/250	9.474
Gd/450	4.200
Ho/700	2.015

Table 4.2: Surface roughness of the thin film samples

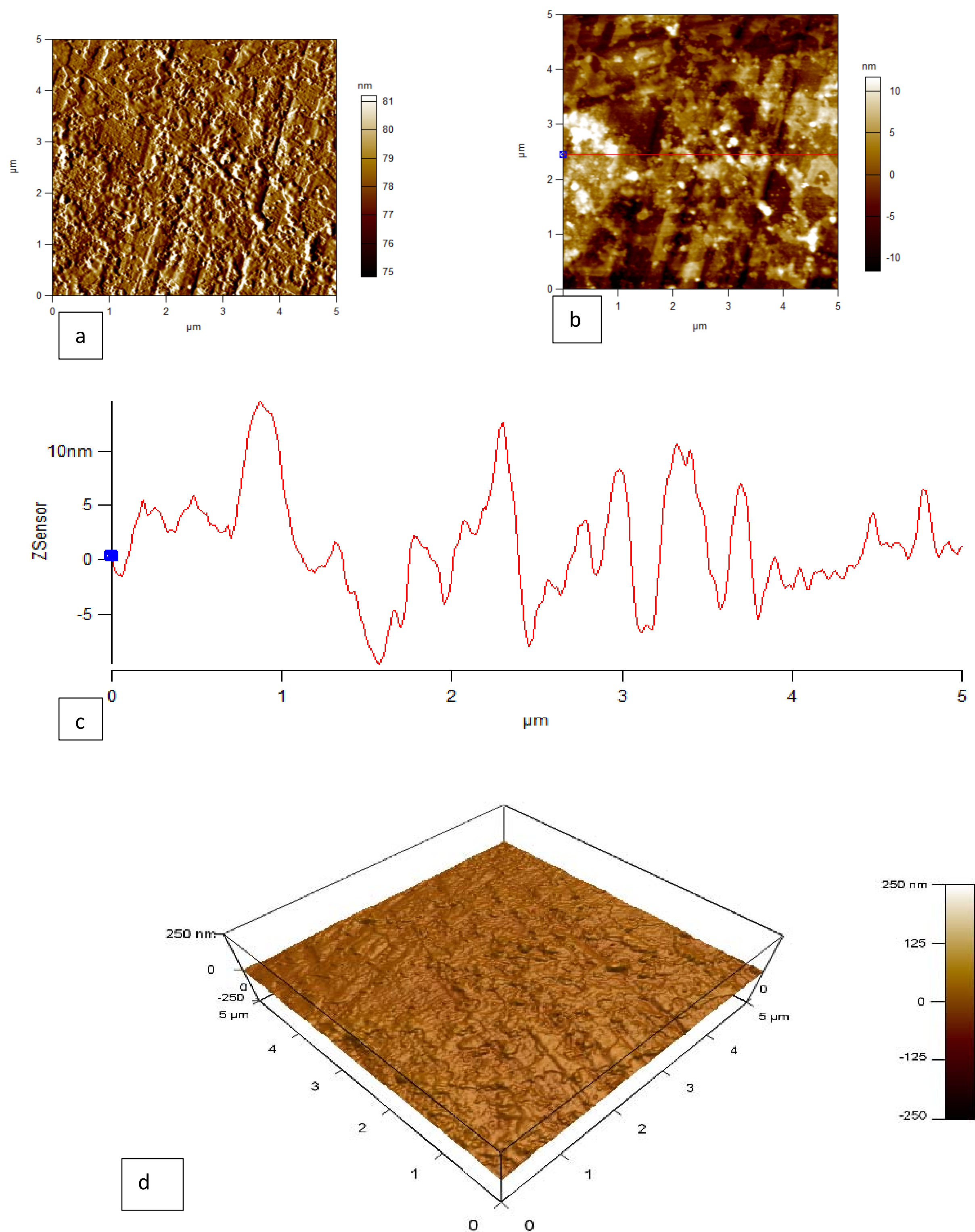

Fig. 4.6: (a) 2-D morphology (b) 2-D sensor retrace (c) Z sensor retrace. (d) 3-D morphology of the sample Sm/-196

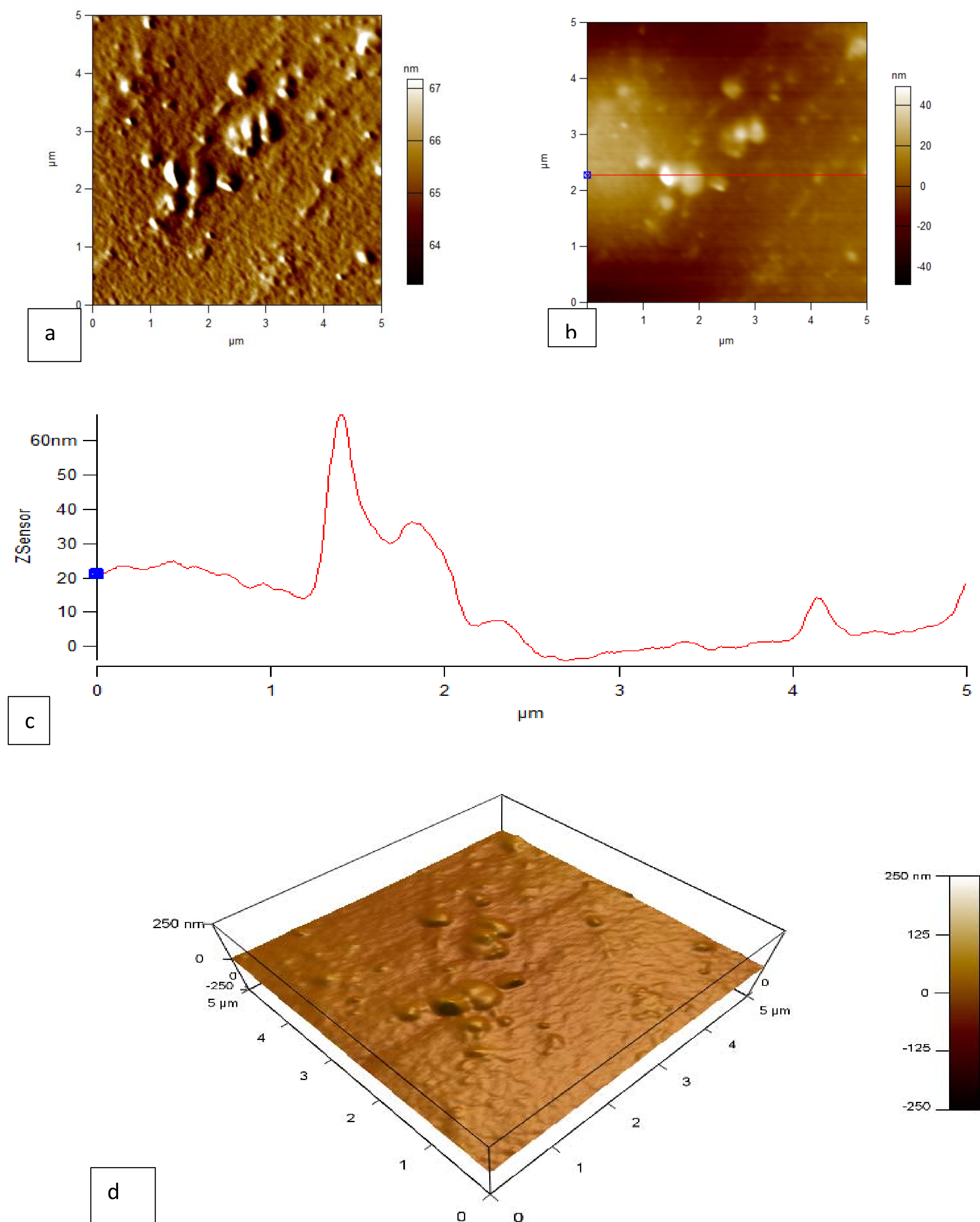

Fig.4.7: (a) 2-D morphology (b) 2-D sensor retrace (c) Z sensor retrace. (d) 3-D morphology of the sample Sm/-196

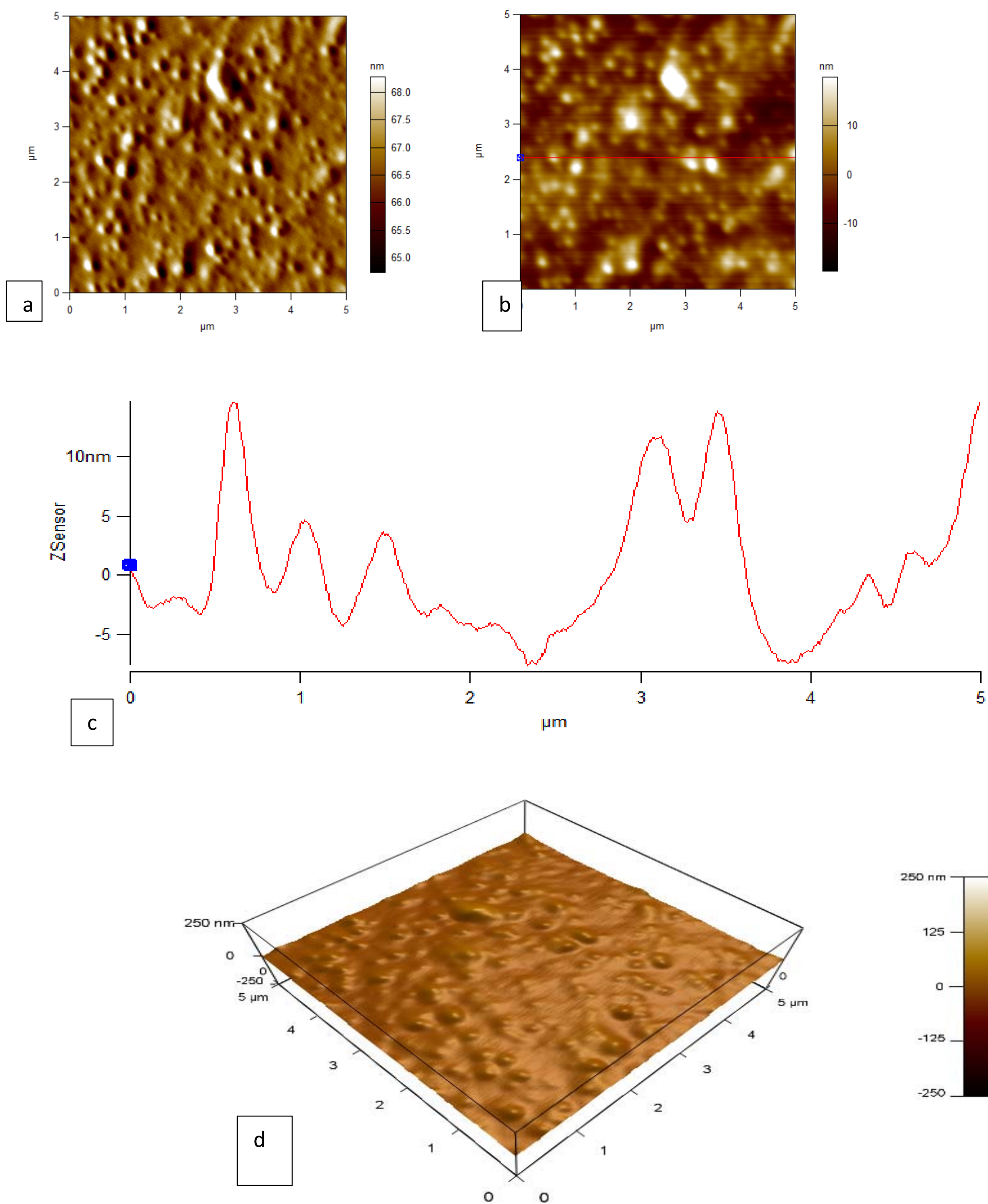

Fig.4.8: (a) 2-D morphology (b) 2-D sensor retrace (c) Z sensor retrace. (d) 3-D morphology of the sample Gd/450

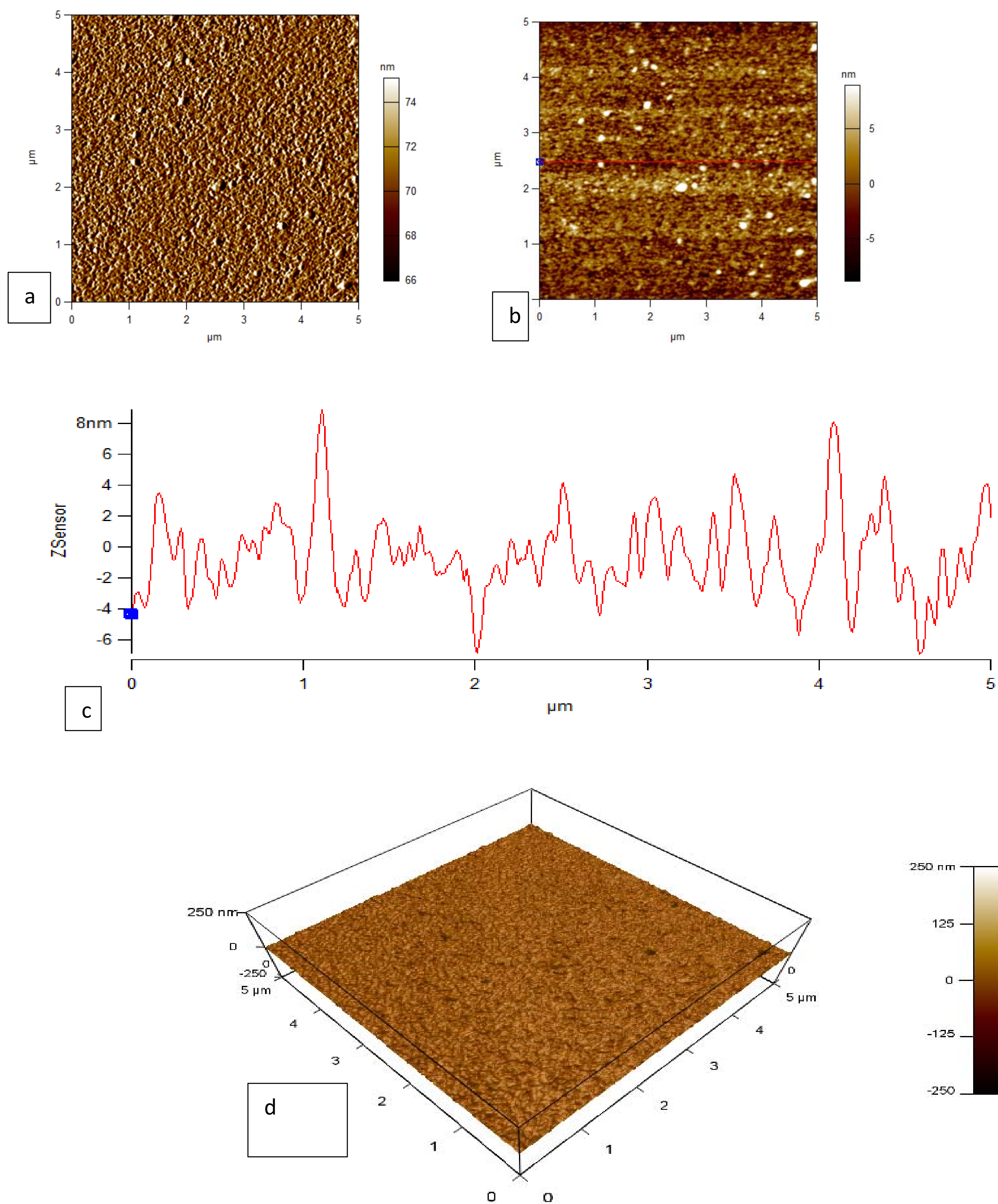

Fig.4.9: (a) 2-D morphology (b) 2-D sensor retrace (c) Z sensor retrace. (d) 3-D morphology of the sample Ho/700

4.1.4 Fourier transform infrared spectroscopy (FTIR)

FTIR measurement is used to identify unknown materials likely to present in the films. IR spectra of the doped films were obtained in transmittance mode with wavenumber range between 400cm^{-1} – 1500cm^{-1}. The films at all deposited temperatures exhibited IR spectral characteristic of aluminum nitride.

Figures 4.10 a-d below are IR spectra for the samples Sm/-196, Gd/250, Gd/450 and Ho/700 respectively. They show characteristic infrared active modes of Aluminum nitride. All films show absorption peaks between 390cm^{-1} – 500cm^{-1}, which is vibration mode for rare-earth metals-oxygen bond.[20,21]

Films deposited at high temperatures (Figs. 4.10 b-d) show others peaks at ranges 770cm^{-1} – 900cm^{-1} which is vibration mode for Si-N bond and 1035 - 1150cm $^{-1}$ which is vibration (stretching) mode for Si-O-Si. The formation of Si-N and Si - O – Si in films with high deposition temperature might likely be relating to substrate high temperature results in bonding of silicon substrate and nitrogen as well as oxidation of the silicon.

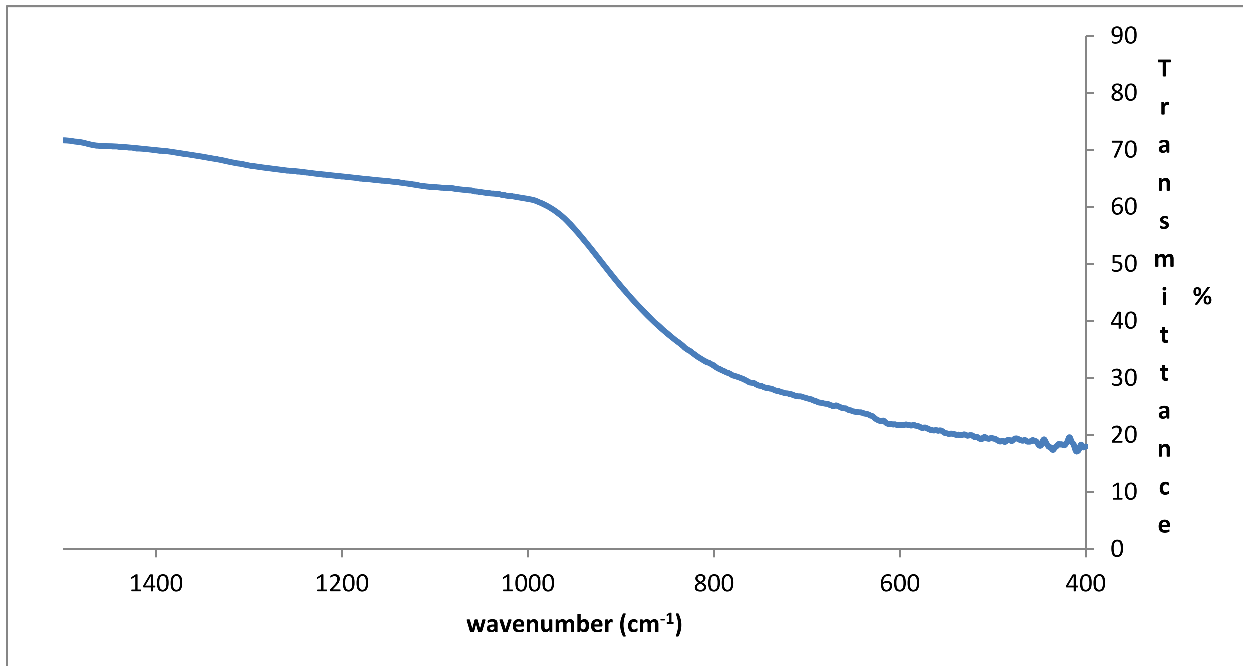

Fig. 4.10a: FTIR graph of sample Sm/-196

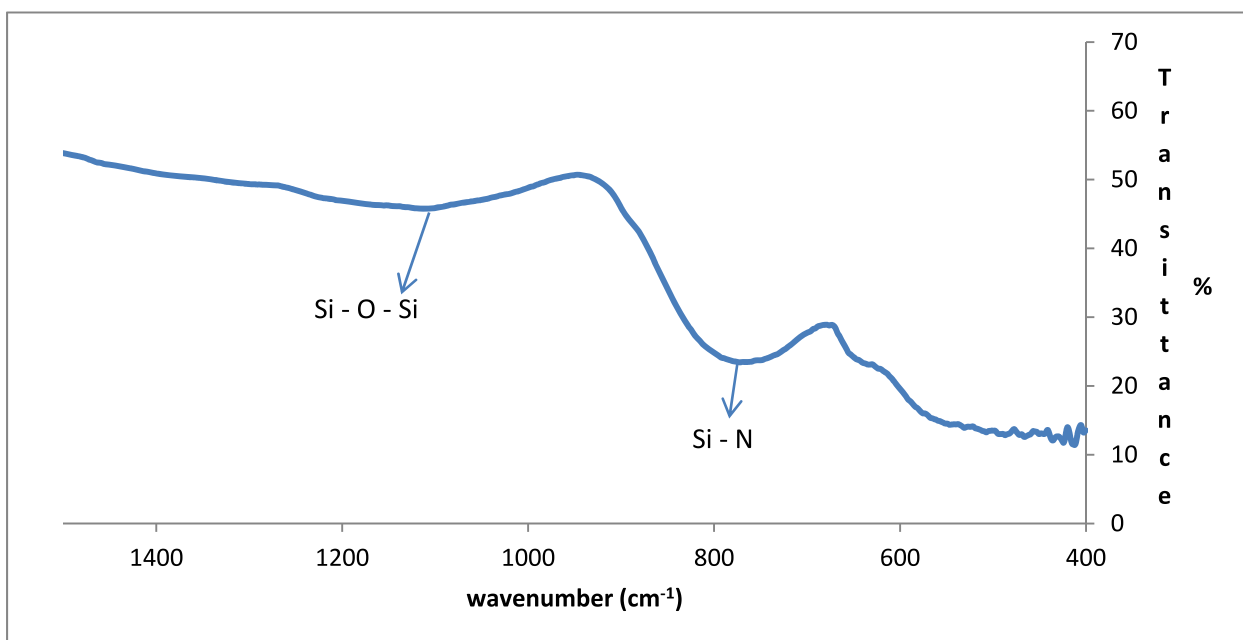

Fig.4.10b: FTIR graph of sample Gd/250

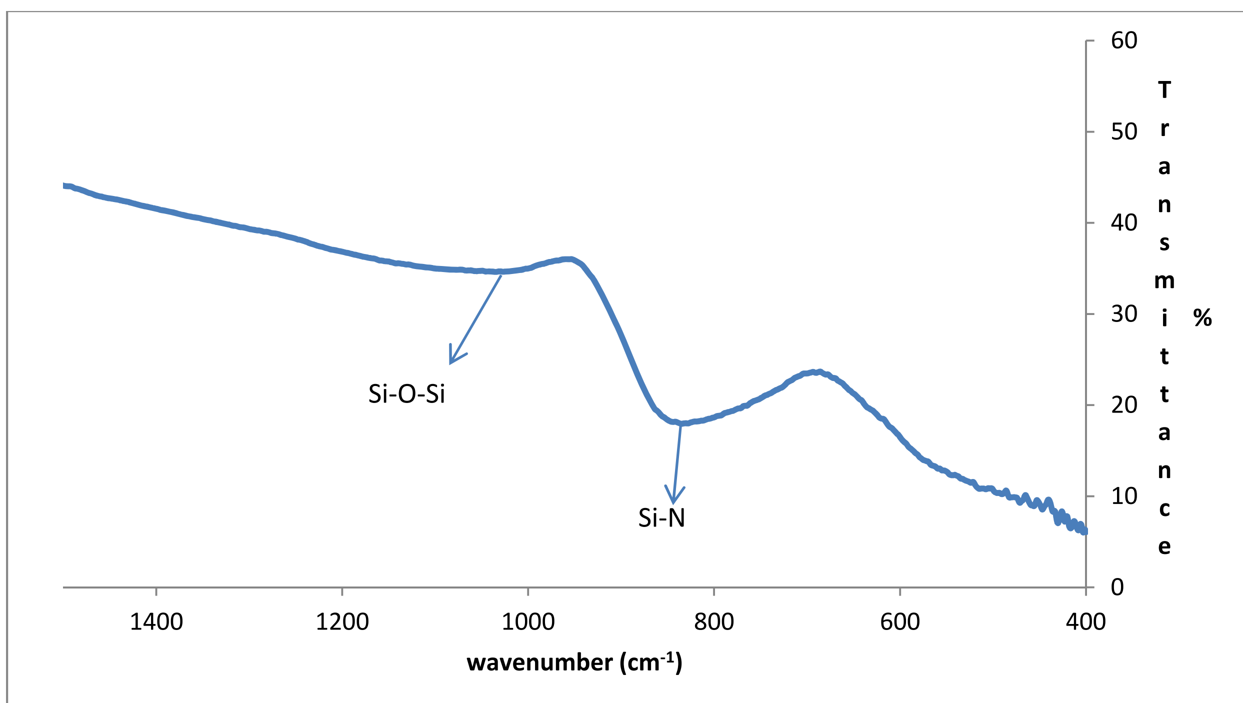

Fig.4.10c: FTIR graph of sample Gd/450

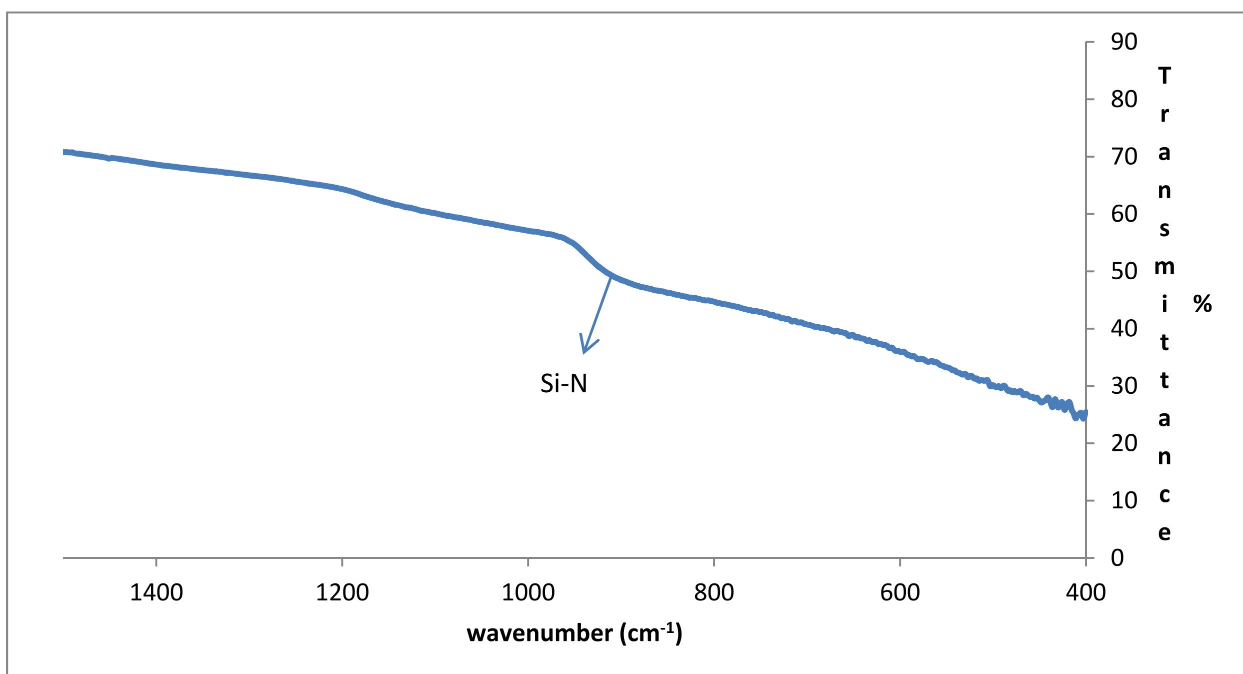

Fig.4.10d: FTIR graph of sample Ho/700

4.1.5 Thermo gravimetric analysis

The non-isothermal degradation of doped AlN thin films have been investigated by TGA. The results are shown in Figs. 4.11 a-d below. All films are relatively stable by losing less than 10% of their total masses between 100°C and 900°C.

Sample Sm/-196 deposited at 77K with samarium lost highest mass of around 7% within the heating range, then follow by the sample Ho/700 deposited at 700°C with holmium and the other samples Gd/250 and Gd/450 with gadolinium are relatively the same. Being amorphous or crystalline might not affect thermal stability of the AlN films.

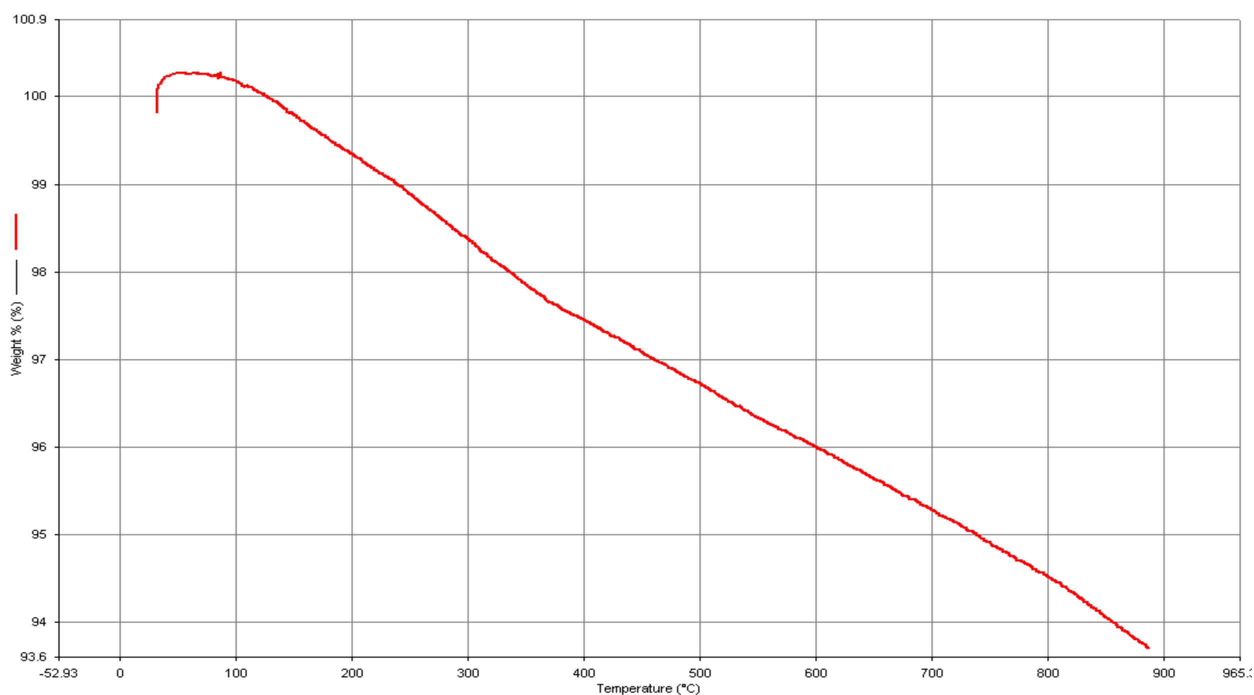

Fig. 4.11a: TGA graph of the sample Sm/-196

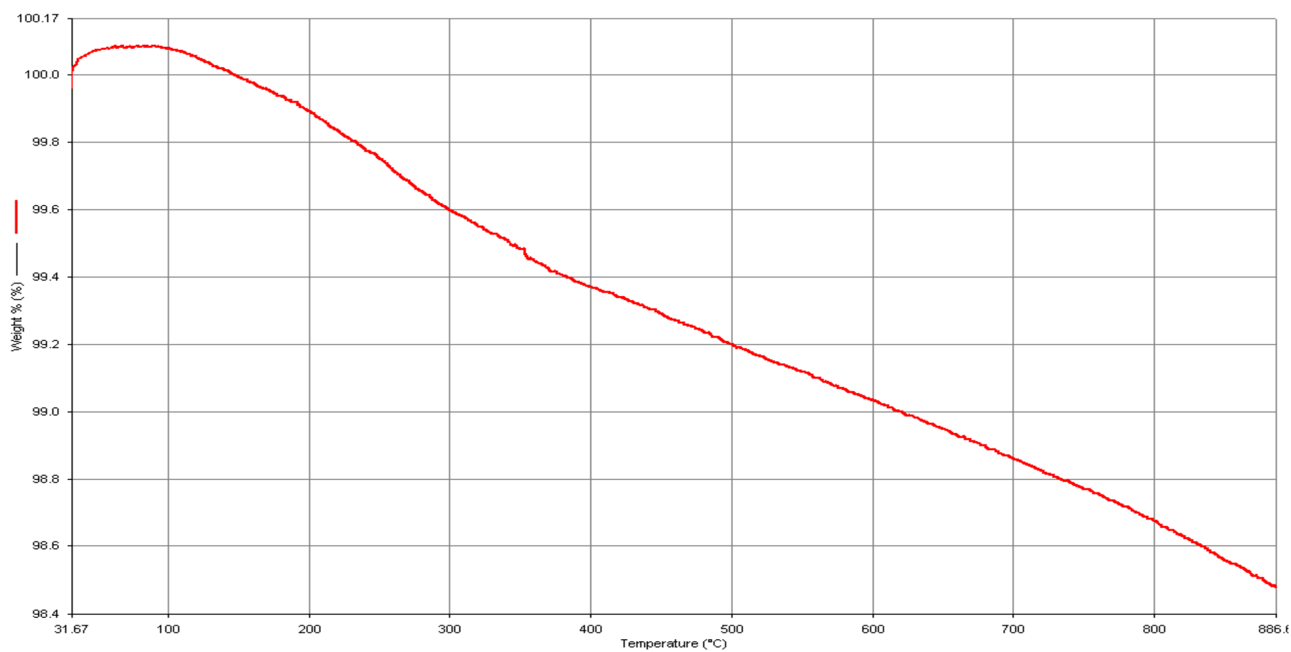

Fig. 4.11b: TGA graph of the sample Gd/250

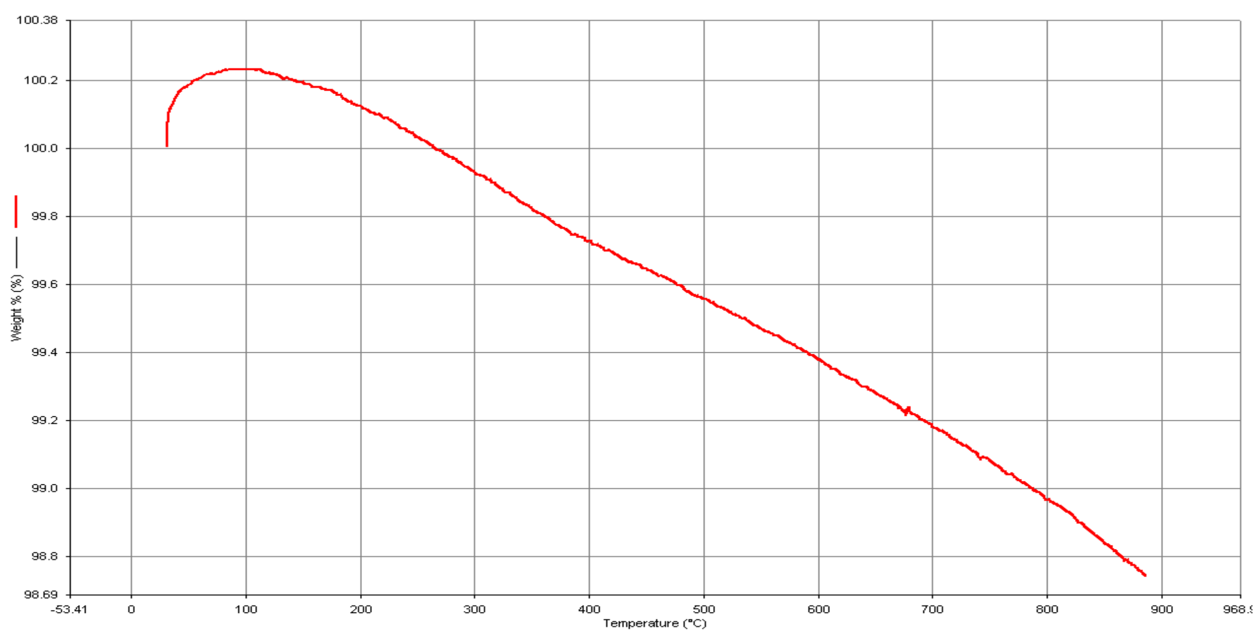

Fig. 4.11c: TGA graph of the sample Gd/450

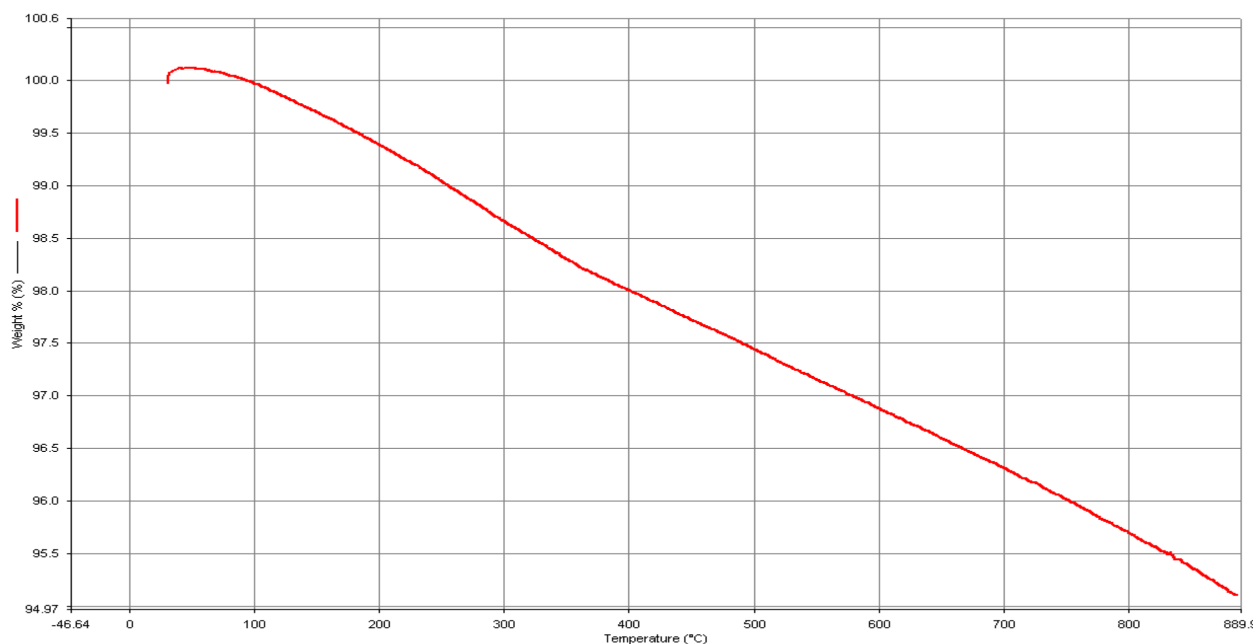

Fig.4.11d: TGA graph of the sample Ho/700

4.2 Luminescence

4.2.1 Photoluminescence

Photoluminescence is divided into two categories: fluorescence and phosphorescence. “A pair of electrons occupying the same electronic ground state having opposite spins and are said to be in a singlet spin state (Fig. 4.12a) When an analyte absorbs an ultraviolet or visible photon, one of its valence electrons moves from the ground state to an excited state with a conservation of the electron’s spin (Fig. 4.12b). Emission of a photon from the singlet excited state to the singlet ground state—or between any two energy levels with the same spin—is called fluorescence. The probability of fluorescence is very high and the average lifetime of an electron in the excited state is only 10^{-5}–10^{-8} s. Fluorescence, therefore, decays rapidly once the source of excitation is removed.”

In some cases an electron in a singlet excited state is transformed to a triplet excited state (Fig. 4.12c) in which its spin is no longer paired with the ground state. Emission between a triplet excited state and a singlet ground state—or between any two energy levels that differ in their respective spin states is called phosphorescence. Because the average lifetime for phosphorescence ranges from 10^{-4}–10^{4} s, phosphorescence may continue for some time after removing the excitation source.[31]

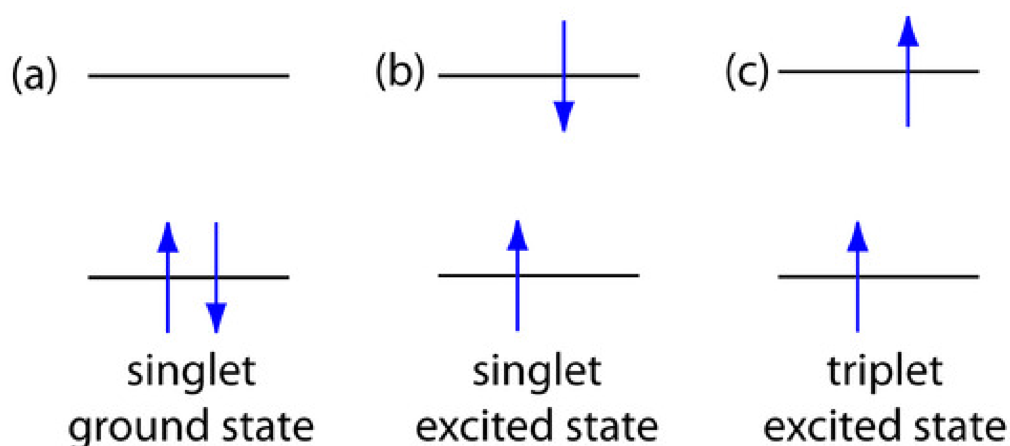

Figure 4.12: Electron configurations for (a) a singlet ground state; (b) a singlet excited state; and (c) a triplet excited state.

"The choice of excitation is critical in any PL measurement. The excitation energy and intensity will have profound effects on the PL signal. Although the excitation conditions must be considered carefully, the strength of the PL technique relies heavily on the flexibility that these adjustable parameters provide. Because the absorption of most materials depends on energy, the penetration depth of the incident light will depend on the excitation wavelength. Hence, different excitation energies probe different regions of the sample. The excitation energy also selects the initial excited state in the experiment. Because lasers are monochromatic, intense, and readily focused, they are the instruments

of choice for photoluminescence excitation (PLE). For many applications, the excitation energy is not critical.[19]"

"The absorption of a material depends strongly on the energy of the incident light. In the analysis of surfaces, it is useful to describe this wavelength-dependent absorption by a penetration depth (the inverse of the absorption coefficient), which is a measure of the thickness of the layer that is probed.[22]"

PL studies of films deposited on flat silicon substrate were performed at room temperature. Films were excited by laser beam of 532nm with power of 125mW and high voltage of 900V. The beam focused on sample surface by objective lens, the focused beam excited atom of the sample and sample emits PL light. The objective lens collimates the light and focused to fiber by focus lens. The fiber delivers the PL light to spectrometer for detection within range 500nm – 850 nm. Generally, three kinds of spectra are generally measured, which provide complementary information, but in this work only luminescence or emission spectra are recorded by scanning the monochromator, which analyses energy emitted from the sample under fixed excitation conditions. In general the emitted photon energy is lower (wavelength higher) than the excitation energy (Stokes' law). [8, 15,28].

Emission spectra are presented as graphs of intensity versus (emission) wavelength. Generally the intensity is presented in terms of arbitrary units instead of radiometric absolute values. Abscissa units for wavelength is nanometers.[28]

Figures 4.12, 4.13, and 4.14 show room temperature PL emissions from sample Sm/-196, sample Ho/700 and AlN: Tm films respectively.

Sample	Laser power (nm)	Wavelength (nm)	Transition
Sm/-196	532	558.0	$^4G_{5/2} \rightarrow {}^6H_{5/2}$
		570.0	$^4G_{5/2} \rightarrow {}^6H_{5/2}$
		606.0	$^4G_{5/2} \rightarrow {}^6H_{7/2}$
Gd/250	532	557.0	$^5S_2 \rightarrow {}^5I_8$
		561.0	$^5S_2 \rightarrow {}^5I_8$
		696.0	$^5I_4 \rightarrow {}^5I_8$
AlN : Tm	530	611.5	$^3F_2 \rightarrow {}^3H_6$
		810.7	$^3H_4 \rightarrow {}^3H_6$
AlN : Tm	783	802.6	$^3H_4 \rightarrow {}^3H_6$
		812.6	$^3H_4 \rightarrow {}^3H_6$

Table 4.3: Photoluminescence results of the samples

Photoluminescence results show both doped amorphous and crystalline films emit photon at visible region. The quality of the host does not affect the luminescence properties of these rare earth elements.

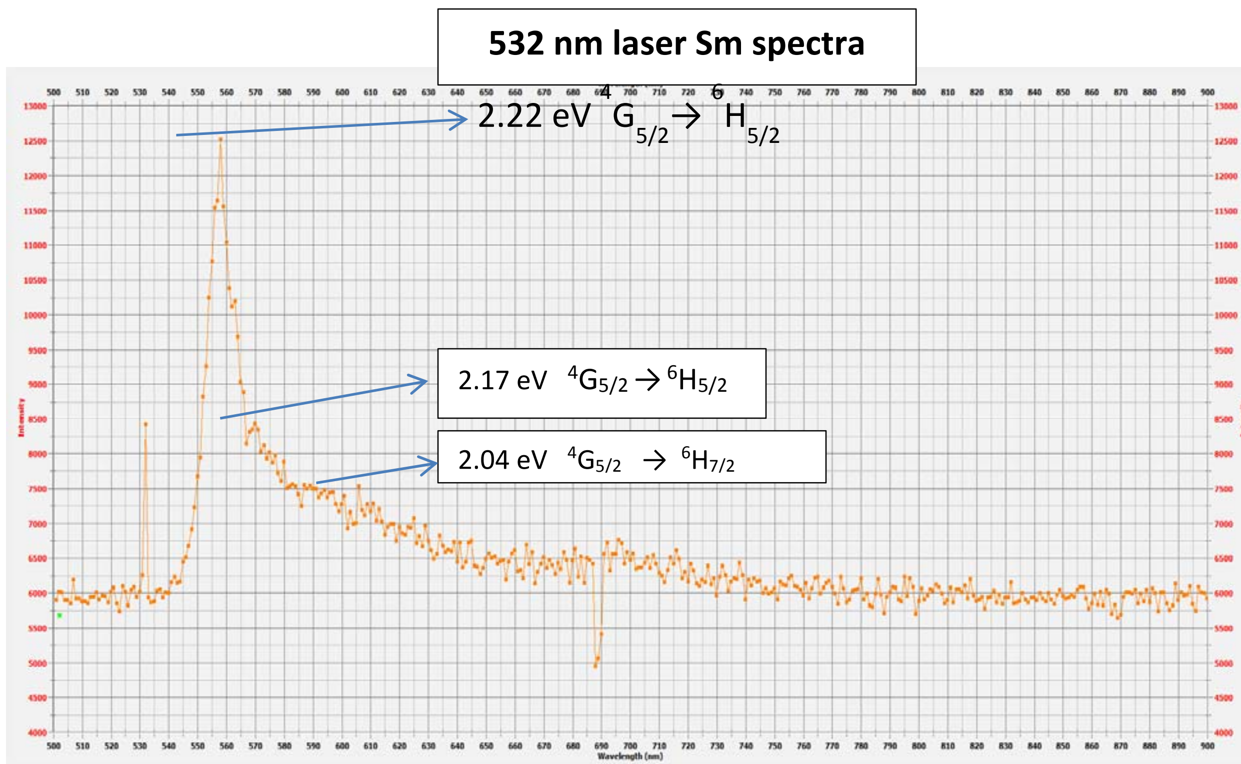

Fig. 4.13: Photoluminescence spectrum of sample Sm/-196 excited with 532 nm laser

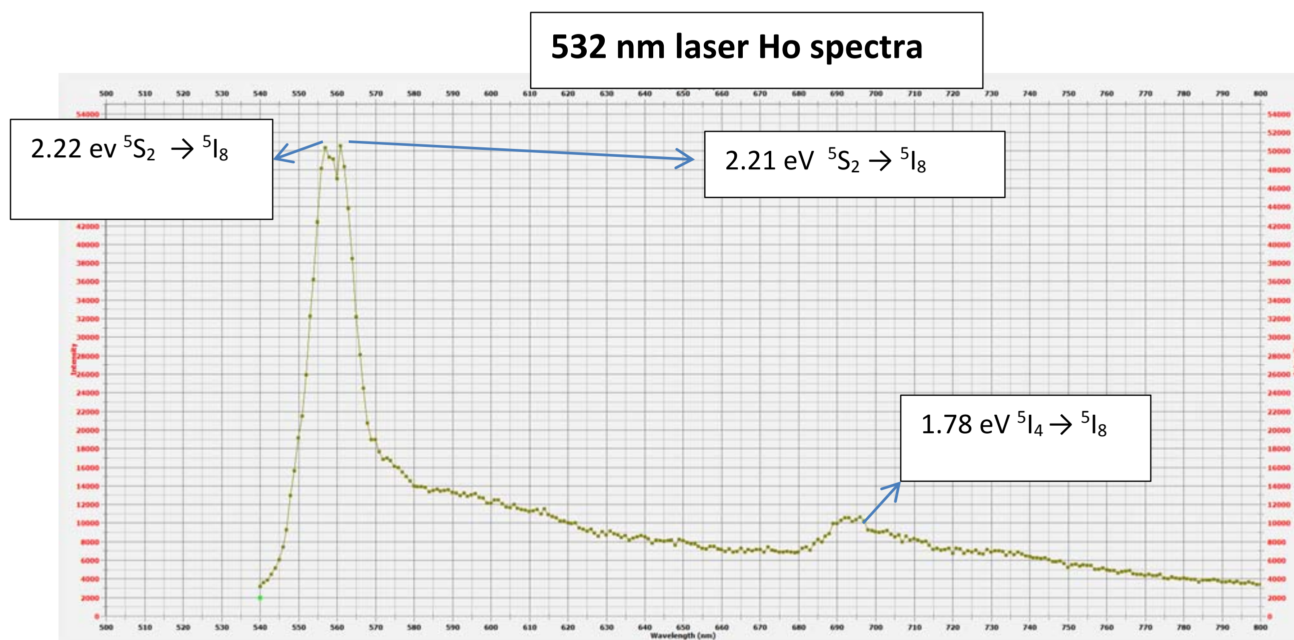

Fig. 4.14: Photoluminescence spectrum of sample Ho/700 excited with 532 nm laser

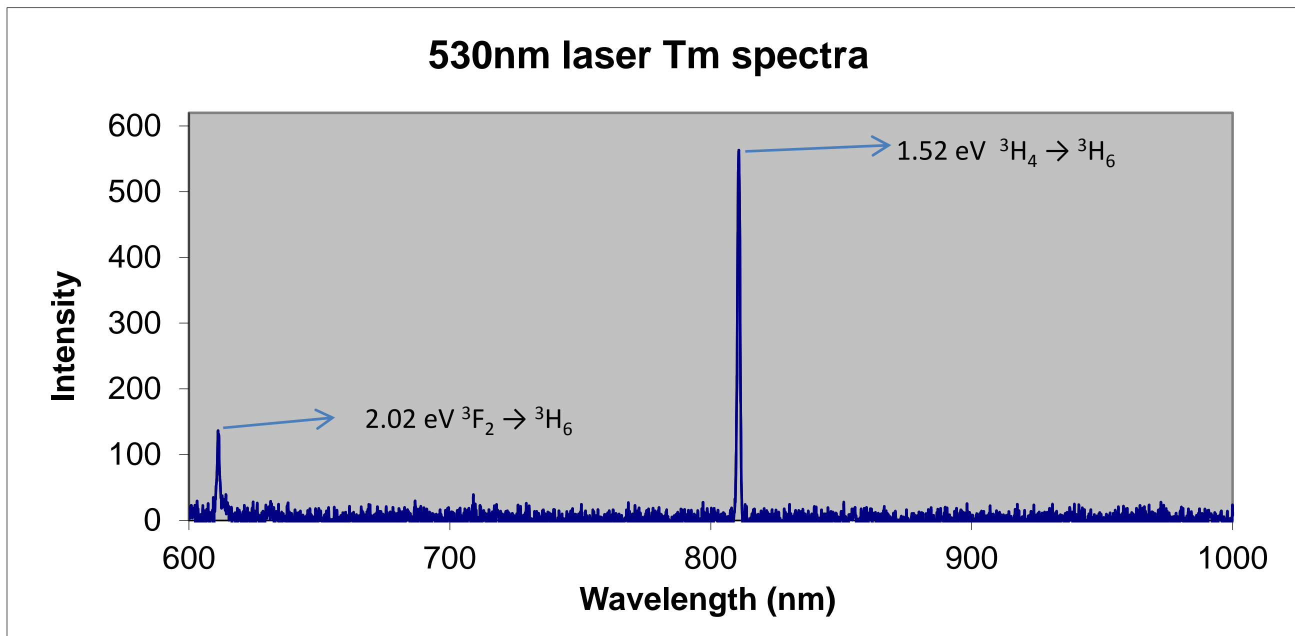

Fig. 4.15: Photoluminescence spectrum of AlN: Tm excited with 530 nm laser performed at Ball state university Indiana, USA

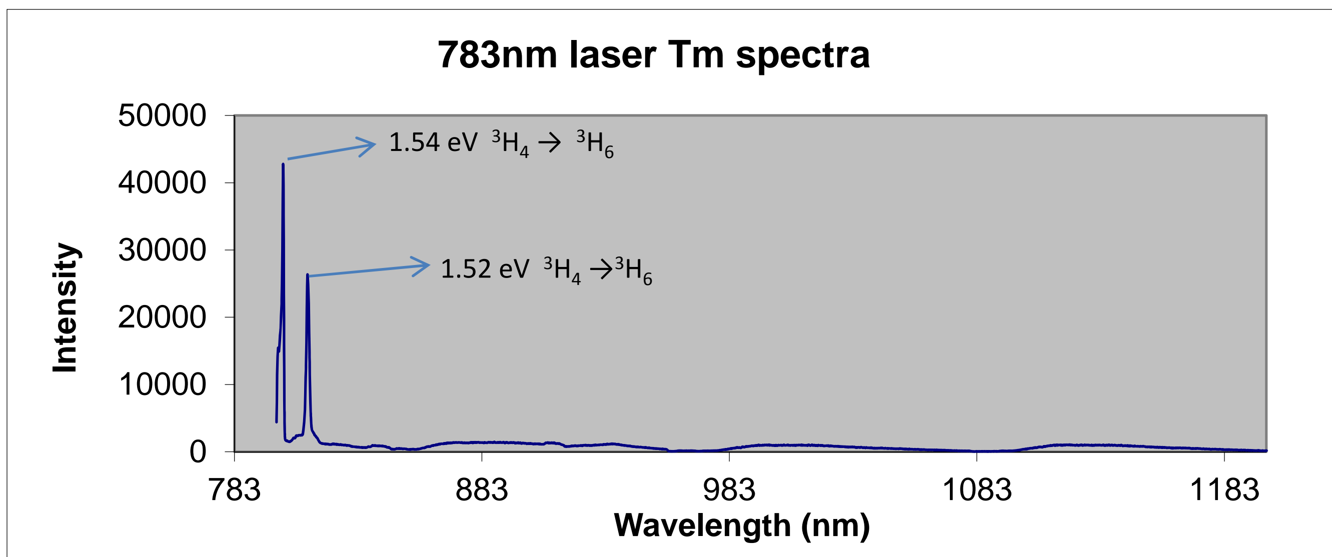

Fig. 4.16: Photoluminescence spectrum of AlN: Tm excited with 783 nm laser performed at Ball state university Indiana, USA.

Chapter 5

Conclusions

In the present work, surface characterization and luminescence properties of aluminum nitride thin films doped with rare-earth elements, Sm, Gd, Ho and Tm have been studied.

RF magnetron sputtering, X-ray diffraction (XRD), Scanning electron microscopy (SEM) /Energy dispersive X-ray (EDAX), Atomic force microscopy (AFM), Fourier transform infrared (FTIR), Thermal gravimetric analysis (TGA) and photoluminescence (PL) tool are used for the growth, characterization and luminescence property.

Films were deposited at different growth temperature on substrates. Liquid nitrogen was used during the growth of -196°C to cool the substrates and amorphous films were obtained. Electric heater was used to keep substrates at high temperature for crystalline films.

SEM, XRD and AFM gave information about the structure of the films, FTIR revealed information about sub-surface bonds and TGA gave thermal stability information.

All samples were investigated for their luminescence using photon excitation. Emission spectra were obtained for all materials under investigation except one with gadolinium, (Gd) , which has its own at ultraviolet region. The most probable and well know $4f - 4f$ energy level transitions of rare-earth ions were used to assign transitions that occurred during photoluminescence as shown in luminescence spectra and emission lines of all investigated doped films. Samarium and holmium were giving transitions in the low energy portion of the visible spectrum and thulium is found to be a good orange and IR emitter.

Future work

Further work is needed to study the effect of growth temperature on the mechanical and chemical properties as well as refractive index of the samples investigated. In addition, the more reliable quantitative analysis could be done by using ICP-MS tool and surface area measurements of the films. People can exploit these ideas and results for the construction of solid state laser and LED.

References

1. M. Maqbool *et al,* Cathodoluminescence from Amorphous and Nanocrystalline Nitride Thin Films doped with Rare Earth and Transition Metals, Dr. Naoki Yamamoto (Ed.), In-Tech, 2012,
2. N. Kumari *et al*, Study of properties of AlN thin films deposited by reactive magnetron Sputtering, Int. J. Thin Fil. Sci. Tec. 3, No. , 43-49 (2014).
3. R. D Vispute *et al*, Epitaxial growth of AlN thin films on Silicon (111) substrates by Pulsed Laser deposition, J. Appl. Phys., Vol.77, No. 9 (1995).
4. D. S. Dinara, Morphology and structural investigation of Aluminum nitride layers prepared by magnetron sputtering, Doctoral degree programme (2), FEEC BUT.
5. M. Maqbool *et al*, Intense Red Catho- and photoluminescence from 200 nm thick Samarium doped Amorphous AlN thin films, Nanoscale Res. Lett., 2009, 4(7) 748-752.
6. M. Maqbool, Growth, Characterization and Luminescence and optical properties of Rare-earth elements and transition metals doped in wide Band gap Nitride semiconductor, Aug. 2009, Dissertation.
7. H. Morkoc, Nitride Semiconductor and Devices, Springer, Berlin Germany, 1999.
8. D. Zhuang *et al*, Wet etching of GaN, AlN, and SiC: a review, materials science and engineering: R: reports, vol. 48, issue 1, 2005, pages 1 – 46.
9. B. Monemar, Luminescence in III-nitrides, materials science and Engineering B59, 122 (1999).
10. A. H. Kitai (Ed), Solid State Luminescence; Theory, Materials and Devices, Springer, New York, 1993.

11. G. C Yi (Ed), Semiconductor Nanostructures for Optoelectronic Devices: Processing, Characterization and Application; Nanoscience and Technology, Springer, New York, 2012.
12. J.B. Gruber *et al*, J. Appl. Phys., Vol. 91, No. 5 2929-2935 (2002).
13. Research: Nanocharacterization, Nanoscale Devices and Materials Physics laboratory 2005 – 2013, Department of Physics, Sungkyun kwan University Sunwon Korean.
14. A. J. Kenyon, Recent Developments in Rare-earth doped materials for optoelectronics: Review, Progress in Quantum Electronics, 26 (2002) 225-284.
15. P. Hannian *et al*, Lanthanide Luminescence; Photophysical, Analytical, Biological Aspects; Springer, Berlin Germany, 2011.
16. H. J. Joo *et al*, The optical and structural properties of AlN thin films characterized by spectroscopic ellipsometry, Thin solid films, 368 (2000) 67-73.
17. M. A. Auger *et al*, Structure and morphology evolution of AlN films grown by DC sputtering, Surf. and coating tech., 180 – 181 (2004) 140 – 144.
18. N. Matsunami *et al*, XRD Characterization of AlN Thin films prepared by reactive RF- sputter deposition, Adv. In mats. Phys. and chem., 2013, 3, 101 – 107.
19. S. M. Norazlina *et al*, Structural and optical properties of Chromium doped AlN thin films prepared by stacking of Cr layer on AlN thin film, Int. J. of Eng. Trends and Tech.,-Vol. 9 Number 13 (2014).
20. E. Tomaszewics *et al*, New Cadmium and rare-earth metal molybdates with scheelite-type structure, mats. Chem. and phys., 122 (2010) 595-601.
21. F. Wieslawa *et al*, Spectral and thermal behaviuors of rare earth element complexes with 3,5- dimethoxybenzoic acid, J. Serb. Chem. Soc., 68(10)751-763(2003).

22. T. H. Gfroerer, Photoluminescence in Analysis of Surfaces and Interfaces, Encyclopedia of Analytical Chemistry, pg.9209-9231, John Wiley & sons Ltd, Chi Chester, 2000.

23. Y. Weseda et al, X-ray Diffraction Crystallography; Introduction, Examples and Solved problems, Springer, New York, 2011.

24. A. H. Kitai (Ed), Solid State Luminescence; Theory, Materials and Devices, Springer, New York, 1993.

25. G. C Yi (Ed), Semiconductor Nanostructures for Optoelectronic Devices: Processing, Characterization and Application; Nanoscience and Technology, Springer, New York, 2012.

26. G. Liu et al (eds), Spectroscopic Properties of Rare earths in Optical Materials, Springer, New York, 2005.

27. S. Adachi, Optical properties of Crystalline and Amorphous Semiconductors; Materials and Fundamental Principles, Springer, New York, 1999.

28. D. R. Vij, Luminescence of Solids, Springer, New York, 1999.

29. K. K. Nanda *et al*, Measurement of surface roughness by atomic force microscopy and Rutherford backscattering spectrometry of CdS nanocrystalline films, Appl. Surf. Sci., 133 (1998) 293-297.

30. Synthesis and Characterization of nanostructures.

31. D. Harvey, Photoluminescence Spectroscopy, Chemwiki.

32. P. P. Mondal *et al*, Fundamentals of Fluorescence microscopy, Springer, Berlin Germany, 2013.

33. B. E. Warren, X-ray diffraction, Addison-Wesley, Reading, 1969.

34. R. R. L. De Oliveira *et al*, Measurement of the Nanoscale Roughness by Atomic Force

Microscopy: Basic principles and Applications, Atomic Force Microscopy – Imaging, Measuring and Manipulating Surfaces at the atomic scale, Dr. Victor Bellitto (Ed), 2012, Intec.

35. J. Ibanez *et al*, Far- infrared transmission in GaN, AlN, and AlGaN thin films grown by Molecular Beam Epitaxy, J. of Appl. Phys, 104, 033544 (2008).

36. R.E. Hummel, Electronic properties of materials, fourth edition, Springer, Berlin Germany 2010.

37. R. Bosco *et al*, Surface Engineering for Bone Inplants: A Trend from Passive to Active Surfaces, Coatings, Vol. 2, Issue 3, 2012.